AD-A067 758 SYRACUSE UNIV NY DEPT OF ELECTRICAL AND COMPUTER EN--ETC F/G 20/3
THE CAPACITANCE OF DISCS OF ARBITRARY SHAPE.(U)
APR 79 E E OKON, R F HARRINGTON N00014-76-C-0225
UNCLASSIFIED TR-79-3 NL

END
DATE FILMED
6-79
DDC

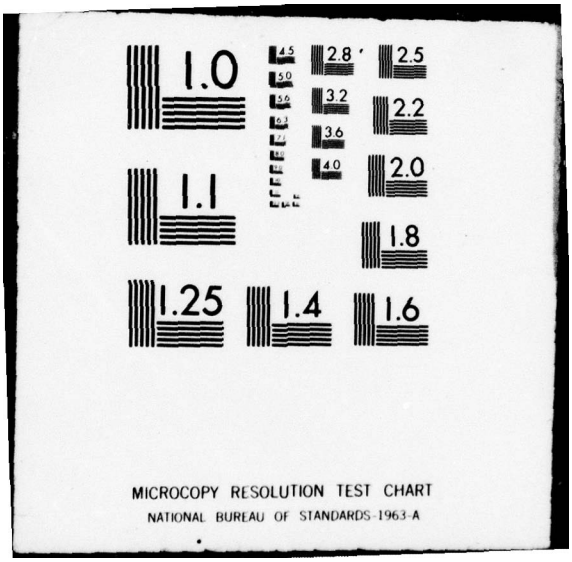
1.0
1.1
1.25
1.4
1.6
1.8
2.0
2.2
2.5
2.8
3.2
3.6
4.0
4.5
5.0
5.6
MICROCOPY RESOLUTION TEST CHART
NATIONAL BUREAU OF STANDARDS-1963-A

UNCLASSIFIED

SECURITY CLASSIFICATION OF THIS PAGE (When Data Entered)

REPORT DOCUMENTATION PAGE	READ INSTRUCTIONS BEFORE COMPLETING FORM
1. REPORT NUMBER: TR-79-3, TR-10 (14)	2. GOVT ACCESSION NO.
3. RECIPIENT'S CATALOG NUMBER (9)	
4. TITLE (and Subtitle): THE CAPACITANCE OF DISCS OF ARBITRARY SHAPE . (6)	5. TYPE OF REPORT & PERIOD COVERED: Technical Report No. 10
6. PERFORMING ORG. REPORT NUMBER	
7. AUTHOR(s): Ephraim E. Okon, Roger F. Harrington (10)	8. CONTRACT OR GRANT NUMBER(s): N00014-76-C-0225 (15)
9. PERFORMING ORGANIZATION NAME AND ADDRESS: Dept. of Electrical & Computer Engineering, Syracuse University, Syracuse, New York 13210	10. PROGRAM ELEMENT, PROJECT, TASK AREA & WORK UNIT NUMBERS
11. CONTROLLING OFFICE NAME AND ADDRESS: Department of the Navy, Office of Naval Research, Arlington, Virginia 22217 (11)	12. REPORT DATE: April 1979
	13. NUMBER OF PAGES: 85
14. MONITORING AGENCY NAME & ADDRESS (if different from Controlling Office) (12) 85p.	15. SECURITY CLASS. (of this report): UNCLASSIFIED
	15a. DECLASSIFICATION/DOWNGRADING SCHEDULE

16. DISTRIBUTION STATEMENT (of this Report)

Approved for public release; distribution unlimited.

17. DISTRIBUTION STATEMENT (of the abstract entered in Block 20, if different from Report)

18. SUPPLEMENTARY NOTES

This work was supported in part by a grant from Syracuse University

19. KEY WORDS (Continue on reverse side if necessary and identify by block number)

Arbitrary shapes	Discs
Automatic subdivision	Mesh grading
Capacitance	Method of moments
Charge distribution	Triangular subsections

20. ABSTRACT (Continue on reverse side if necessary and identify by block number)

A method of moments procedure is presented for solving the integral equation satisfied by the electrostatic charge distribution over arbitrary planar domains. This procedure is based on a representation of such domains as a collection of quadrilateral subdomains, using the Gordon-Hall and Zienkiewicz-Phillips subdivision techniques. All integrals are effectively evaluated over triangles, and rely on an expression which is derived for the potential at a point due to a constant charge distribution over a triangular domain. → next page (over)

DD FORM 1 JAN 73 1473 EDITION OF 1 NOV 65 IS OBSOLETE S/N 0102-014-6601

UNCLASSIFIED

SECURITY CLASSIFICATION OF THIS PAGE (When Data Entered)

406 737

As an illustration, the computational procedure is applied to a variety of discs. The computed results are in excellent agreement with the exact values for the circle and the ellipse, and are compared with known numerical values for certain other configurations.

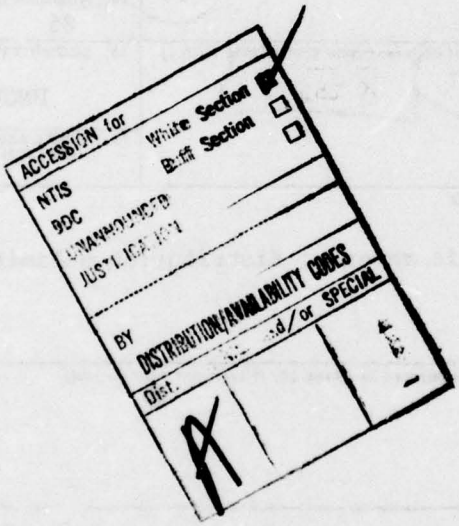

TABLE OF CONTENTS

	Page
PART ONE: THEORY AND RESULTS	
1. INTRODUCTION	1
2. THE INTEGRAL EQUATION AND ITS REDUCTION	2
3. AUTOMATIC SUBDIVISION PROCEDURES	4
3.1. Introduction	4
3.2. The Zienkiewicz-Phillips Technique	7
3.2.1. A Procedure for Subdividing a Single Zone	7
3.2.2. Applications of the Z-P Procedure	10
3.3. The Gordon-Hall Procedure	11
3.4. Mesh-Grading Features	14
3.4.1. The Gordon-Hall Square	14
3.4.2. The Zienkiewicz-Phillips Square	18
3.5. Applications of the Automatic Procedures	20
3.5.1. The Quadrilateral	20
3.5.2. The Triangle	22
3.5.3. The Ellipse	24
3.5.4. The Ellipse Sector	26
3.5.5. The Circle with Two Tangents	27
3.5.6. The Annulus Sector	29
3.5.7. Contours Defined by a Set of Points	30
4. THE INTERACTION MATRIX AND THE POTENTIAL INTEGRAL	35
4.1. Integration over Triangular and Quadrilateral Domains	35
4.2. The Potential due to a Uniform Charge Distribution over a Triangular Domain	39
5. RESULTS AND OBSERVATIONS	43
5.1. Charge Distribution	43
5.2. Capacitance	51
6. CONCLUSION	56
REFERENCES	64

Page

APPENDIX---------- 67

A.1. The Capacitance of an Ellipsoid---------- 67
A.2. The Potential due to a Unifrom Charge Distribution over a Triangle---------- 68

A.2.1. Field Points in the Plane of the Triangle------ 69

A.2.1.1. The ξ-Integral---------- 69
A.2.1.2. The η-Integrals---------- 70

A.2.2. Arbitrary Field Points---------- 73

A.2.2.1. The ξ-Integral---------- 73
A.2.2.2. The η-Integral---------- 73
A.2.2.3. Planar Interactions---------- 80

1. INTRODUCTION

The problem of determining the charge distribution on a perfectly-conducting flat disc, and hence the capacitance of such a disc, is a classical one. By dividing a square plate into square subsections, Maxwell obtained a numerical solution of the integral equation satisfied by the charge density. A similar method (i.e. the method of square subareas) was used by Reitan and Higgins [2] and Harrington [3] to determine the capacitance of rectangular plates. A numerical solution using a variational approach has been considered by Noble [4]. However, the method of square subareas is obviously not ideal for plates of arbitrary shape. The present report describes a numerical procedure for solving the integral equation satisfied by the charge density on an arbitrarily-shaped disc, and hence for determining its capacitance.

The method employs a method of moments approach in which the charge distribution on the disc is approximated by pulses defined over quadrilateral subdomains. These subdomains are generated automatically either by the use of the Zienkiewicz-Phillips isoparametric coordinate procedure [5], or through the use of the transfinite blending transformations of Gordon and Hall [6]. An advantage of the use of quadrilateral subdomains is that fewer expansion functions are required, compared to a method of moments procedure based on triangular subdomains. The method described is applied a variety of discs.

2. THE INTEGRAL EQUATION AND ITS REDUCTION

The charge density $\sigma(x,y)$ on the disc Ω satisfies the well-known singular integral equation

$$\frac{1}{4\pi\varepsilon_o} \iint_{\Omega} \frac{\sigma(x,y)d\Omega}{D} = V \quad , \tag{1}$$

where V is the constant electric potential on the disc, ε_o the permittivity of free space and $D = D(x',y';x',y')$ the distance between the source point (x,y) and the field point (x',y'), is given by

$$D = [(x' - x)^2 + (y' - y)^2]^{1/2} \quad .$$

By dividing the disc Ω into n quadrilateral subdomains Ω_r , r = 1,2,...,n, and defining n pulse expansion functions

$$f_r(x,y) = 1, \quad (x,y) \in \Omega_r, \quad f_r(x,y) = 0, \quad (x,y) \notin \Omega_r,$$
$$r = 1,2,\ldots,n,$$

the unknown charge distribution can be represented approximately as

$$\sigma(x,y) = \sum_{r=1}^{n} A_r f_r(x,y) \quad , \tag{2}$$

where the A_r are constants to be determined. If we now insert (2) in (1) and apply a point-matching procedure to determine the potentials at the n points $(x_s' , y_s') \in \Omega_s$, s = 1,2,...,n, we obtain a system of n simultaneous equations:

$$\sum_{r=1}^{n} C_{sr} A_r = V , \tag{3}$$

$s = 1,2,\ldots,n,$

where

$$C_{sr} = \frac{1}{4\pi\varepsilon_o} \iint_{\Omega_r} \frac{dxdy}{D(x', y'; x,y)} . \tag{4}$$

Once the interaction matrix $[C_{sr}]$ is determined, the constants A_r are readily obtained by solving (3), so that the charge density $\sigma(x,y)$ is found from (2).

In order to evaluate the integral in (4), the quadrilateral Ω_r is subdivided into four triangles having the match-point (x_r' , y_r') ε Ω_r as a common vertex, the integral being evaluated piecewise so that

$$C_{sr} = \frac{1}{4\pi\varepsilon_o} \sum_{k=1}^{4} C_{srk} , \tag{5a}$$

where

$$C_{srk} = \iint_{\Omega_{rk}} \frac{dxdy}{D(x_s' , y_s' ; x,y)} \tag{5b}$$

Thus the calculation of the couplings C_{sr} depends ultimately on (i) the choice of the subdomains Ω_r and (ii) the evaluation of integrals of the type appearing in (5b).

If Δ_{rk} is the area of triangle Ω_{rk}, then using (2), an estimate of the capacitance of the disc is

$$C = \frac{1}{V} \left(\sum_{r=1}^{n} \sum_{k=1}^{4} A_r \Delta_{rk} \right) .$$

3. AUTOMATIC SUBDIVISION PROCEDURES

3.1. Introduction

In trying to subdivide a domain for a method of moments solution of an electromagnetic field problem, it is important that the subdivision process should involve a minimum amount of data input whilst incorporating at the same time a predetermined flexibility both in the choice of the number of subdomains, as well as in the variation of the density of the match points. Although non-automatic (or manual) subdivision procedures can be applied to any domain, and in particular to simple domains such as the rectangle, the circle, etc., and the parameters describing the domains so generated can then be input into the computer, in practice the amount of labor rapidly becomes prohibitive as the number of the subdomains increases. Besides, the manual method becomes, in effect, a trial-and-error procedure for a domain of arbitrary shape. In order to overcome these problems, the idea of the automatic generation of nodes and subdomains has engaged the attention of many workers, notably those interested in the use of finite element methods.

Research on automatic mesh generation has proceeded along three main fronts. One of these is the technique introduced by Fukuda and Suhara [7] in which the aim is to produce, by a search procedure, a triangulation of the domain of interest in which the triangles are 'well-formed' (i.e. they do not possess angles that are very acute, a triangle shape criteria being defined by a pre-set parameter). In this method the interior nodes are initially generated randomly and

their positions are later modified to exclude triangles which do not meet the shape criterion. This method was later improved by Cavendish [8], the aim being the construction of triangular subdomains whose shapes departed as little as possible from the equilateral. In a very recent improvement, Shaw and Pitchen [9] have succeeded in obtaining a scheme which yields equilateral triangles everywhere in the domain except for some of the triangles which have two of their vertices on the domain boundary.

The second approach is that presented by Zienkiewicz and his co-workers [5,10-13], which uses an isoparametric one-to-one transformation to map a square onto a curvilinear quadrilateral. This method has been extended by them to multiply-connected regions, curved surfaces and three-dimensional domains by the use of zones.

Finally, there is the Gordon-Hall technique [6,14,15] in which the unit square is mapped univalently (i.e. invertibly) onto a given region (together with its boundary). This method, which like that of Zienkiewicz and his school is essentially interpolatory, uses transfinite blending functions so that in mapping the unit square onto the domain of interest, the interpolatory function which extends to the interior of the domain, the function defining the domain boundary, matches this latter function at a non-countable number of points on the boundary. The Gordon-Hall technique of generating curvilinear subdomains is, in this sense, an extension of the Zienkiewicz method.

Apart from the above methods, there are others which use specially-defined natural coordinates and iterative schemes [16], or isoparametric

blending transformations similar to those introduced by Zienkiewicz and Phillips, and Gordon and Hall, but specialized to the generation of three-dimensional meshes [17], as well as a search procedure which aims at triangulating plane polygons [18].

For the computation of the capacitance of discs of arbitrary shape, it is important to choose an automatic mesh generation procedure which incorporates parameters so as to satisfy the following criteria:

(i) there should be a systematic method for identifying and counting the subdomain and their vertices;

(ii) it should be possible to choose from the beginning the number of points at which the charge density is computed, since this choice determines the order of the interaction matrix and can also be used to estimate the capacitance resulting from the use of an infinite number of expansion functions (i.e. the 'asymptotic capacitance');

(iii) allowance should be made as much as possible for the variation of the charge density on the disc, such that more nodes are available near edges (where the charge density becomes infinite) than elsewhere.

Both the Gordon-Hall and Zienkiewicz-Phillips procedures provide the simplest means (based on a Cartesian system) for meeting the first two criteria. By incorporating in them certain modifications which will be described later, automatic procedures satisfying criterion (iii) are derived for dividing a disc of arbitrary shape into quadrilateral subdomains.

3.2. The Zienkiewicz-Phillips Technique

A full treatment of the Zienkiewicz-Phillips mesh generation method is available elsewhere [5,10-12]. We apply the technique here to decompose an arbitrary simply-connected disc whose boundary is determined by a finite number of points. The idea is to divide the disc into a number of zones each of which is defined by eight vertices. Each of these zones is then subdivided into quadrilateral domains in such a way that the zones are connected through those quadrilateral vertices (or nodes) which lie on the inter-zone boundaries.

3.2.1. A Procedure for Subdividing a Single Zone

The square $[-1, 1] \times [-1, 1]$ in the ξ-η plane is mapped invertibly onto the quadrilateral domain ABCD in the x-y plane bounded by four parabolic areas on which eight points lie (Figure 1). These eight points are the images of the points in the ξ-η plane with coordinates $(-1, 1)$, $(0, -1)$, $(1, -1)$, $(1, 0)$, $(1, 1)$, $(0, 1)$, $(-1, 1)$ and $(-1, 0)$, in that order. The points 2, 4, 6, 8 in the x-y plane need not be the midpoints of the sides on which they lie, but must lie within a certain neighborhood of the midpoint [12]. In the mapping, functions $L_i(\xi,\eta)$, $i = 1, 2, \ldots, 8$ are defined such that the position vector of any point P, within or on the piecewise parabolic boundary ABCD can be expressed in the form

$$\underline{r}_P(x,y) = \sum_{i=1}^{8} L_i(\xi,\eta)\, \underline{r}_i(x,y) \ ,$$

where $\underline{r}_1(x,y) = \underline{r}_A$, $\underline{r}_3(x,y) = \underline{r}_B$, etc.

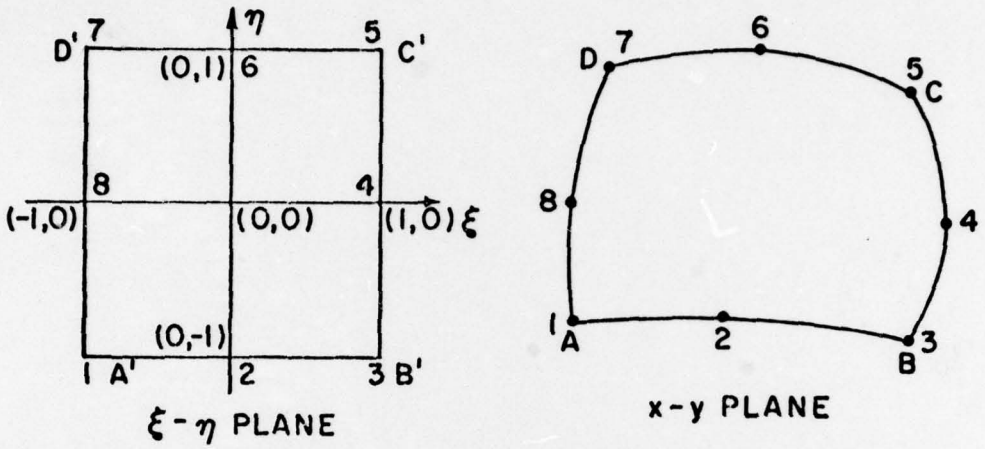

Fig. 1. The Zienkiewicz-Phillips domains.

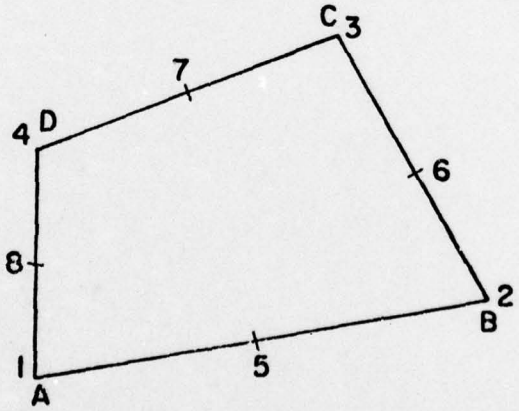

Fig. 2. The image quadrilateral in the x-y plane.

The function $L_i(\xi,\eta)$ are such that $L_i(\xi_j, \eta_j) = \delta_{ij}$, i=1,2,...,8; j=1,2,...,8; where $\delta_{ij} = 1$, i=j

$= 0$, $i \neq j$ (i.e. the Kronecker delta).

They are given by [10]:

$$L_1(\xi,\eta) = -\frac{1}{4}(1-\xi)(1-\eta)(1+\xi+\eta); \quad L_2(\xi,\eta) = \frac{1}{2}(1-\eta)(1-\xi^2);$$

$$L_3(\xi,\eta) = -\frac{1}{4}(1+\xi)(1-\eta)(1-\xi+\eta); \quad L_4(\xi,\eta) = \frac{1}{2}(1+\xi)(1-\eta^2);$$

$$L_5(\xi,\eta) = -\frac{1}{4}(1+\xi)(1+\eta)(1-\xi-\eta); \quad L_6(\xi,\eta) = \frac{1}{2}(1+\eta)(1-\xi^2);$$

$$L_7(\xi,\eta) = -\frac{1}{4}(1-\xi)(1+\eta)(1+\xi-\eta); \quad L_8(\xi,\eta) = \frac{1}{2}(1-\xi)(1-\eta^2). \qquad (6a)$$

By writing $\xi_s = -1 + \frac{s-1}{n_1}$, $s = 1,2,...,2n_1+1$;

$$\eta_t = -1 + \frac{t-1}{n_2}, \quad t = 1,2,...,2n_2+1; \qquad (6b)$$

the square A' B' C' D' is effectively divided into $4n_1\ n_2$ rectangular subdomains such that the arcs AB and CD in the x-y plane are, respectively, divided into $2n_1$ and $2n_2$ segments. The Z-P mapping guarantees, given the condition mentioned earlier, that the image of a point (s,t), with coordinates (ξ_s,η_t), in the ξ-η plane is the unique point P_{st} with coordinates

$$x(\xi_s, \eta_t) = \sum_{i=1}^{8} L_i(\xi_s, \eta_t)x_i;$$

$$x(\xi_s, \eta_t) = \sum_{i=1}^{8} L_i(\xi_s, \eta_t)y_i.$$

3.2.2. Applications of the Z-P Procedure

(i) An Arbitrary Quadrilateral

For the polygon ABCD (Figure 2), taking the four other points required in the Z-P procedure as the midpoints of the sides reduces the parabolic segment of Figure 1 to straight lines segments, and results, on applying (6), in the decomposition

$$\underline{r}_P = \sum_{i=1}^{4} M_i(\xi,\eta)\, \underline{r}_i \ ,$$

where $\underline{r}_1 = \underline{r}_A$, $\underline{r}_2 = \underline{r}_B$, $\underline{r}_3 = \underline{r}_C$, $\underline{r}_4 = \underline{r}_D$, with

$$M_1(\xi, \eta) = \frac{1}{4}(1-\xi)(1-\eta) \ ; \quad M_2(\xi, \eta) = \frac{1}{4}(1+\xi)(1-\eta);$$

$$M_3(\xi, \eta) = \frac{1}{4}(1+\xi)(1+\eta); \quad M_4(\xi, \eta) = \frac{1}{4}(1-\xi)(1+\eta) \ ,$$

and

$$M_i(\xi_j, \eta_j) = \delta_{ij}, \ i,j = 1,2,3,4;$$

$$\underline{r}_A = \underline{r}\,(\xi_1, \eta_1) = \underline{r}(-1, 1), \text{ etc.}$$

(ii) A General Polygon

Consider a general polygon with N vertices. If N is even then the polygon can be divided into p zones, where $p = \frac{1}{2}(N-2)$. If N is odd, then by introducing an extra vertex at the midpoint of the largest side of the polygon, the number of zones is $\frac{1}{2}(N-1)$. A polygon with p zones then has n'vertices', where n=N for N even, and

$n = N+1$ (N odd), and is represented in the ξ-η plane by an in-line arrangement of p squares (Figure 3).

In the x-y plane, zone r has as vertices the points P_r, P_{r+1}, P_{n-r}, $r = 1,2,\ldots, p$, where P_r is the image of the point P'_r in the ξ-η plane. By dividing $P'_r\ P'_{r+1}$ into $2n_1$ segments and $P'_{r+1}\ P'_{n-1}$ into $2n_2$ segments, the entire polygon in the x-y plane is reduced to an array of quadrilateral subdomains determined by $(2n_1p+1) \times (2n_2+1)$ vertices as nodes.

3.3. The Gordon-Hall Procedure

The Gordon-Hall (or G-H) procedure can be applied to domains whose boundaries consist of a finite number of analytically-defined segments through the use of several blending functions [6,14,15]. Recently the blending function method of interpolation has been extended to the semi infinite strip $[0, 1] \times [0, \infty)$ [19]. In the present work we restrict our application of the method to finite simply-connected domains whose boundaries consist of at most four analytically-defined arcs.

In the G-H procedure the unit square A' B' C' D' in the s-t plane (i.e. in the domain S) is to be mapped univalently onto the closed domain R in the x-y plane bounded by the closed curve ABCD so that A, B, C, D are, respectively, the images of A', B', C', and D'. The technique assumes the existence of a continuous vector-valued function $\underline{F}(s,t)$ which maps the s-t plane onto the x-y plane such that the boundary A' B' C' D' is mapped onto the curve passing

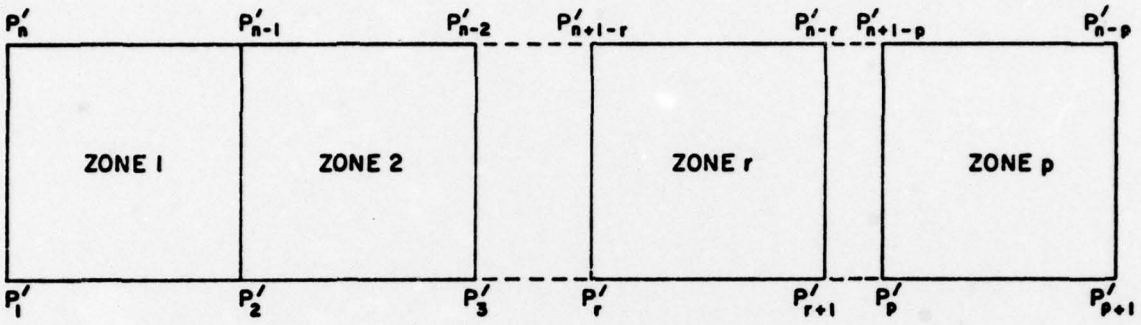

Fig. 3. An in-line arrangement of p Zienkiewicz-Phillips squares.

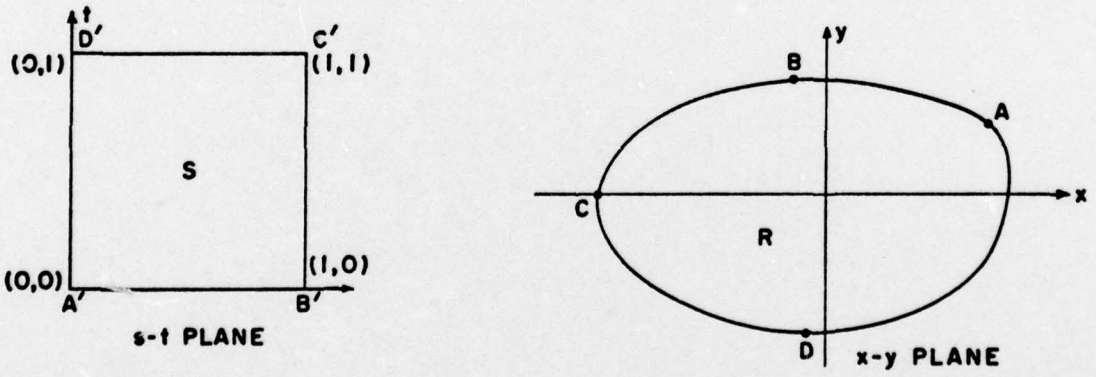

Fig. 4. The Gordon-Hall domains.

through A, B, C, D. A function $\underline{U}$ is then constructed which maps S onto the closed region R in such a way that this function is identical to $\underline{F}(s,t)$ on the boundary of the square. This is due by the introduction of four scalar blending functions

$$\phi_i(s),\ \psi_j(t),\quad i = 0,1;\quad j = 0, 1\ ,\quad \text{defined by}$$

$$\phi_o(s) = 1 - s,\quad \phi_1(s) = s\ ,\qquad 0 \leq s \leq 1\ ;$$

$$\psi_o(t) = 1 - t,\quad \psi_1(t) = t\ ,\qquad 0 \leq t \leq 1.$$

In taking $s_o = 0$, $s_1 = 1$, $t_o = 0$, $t_o = 1$, we have the relations

$$\phi_i(s_k) = \delta_{ik}\ ,\quad \psi_j(t_\ell) = \delta_{j\ell},\quad \begin{cases} i,k = 0, 1; \\ \\ j, \ell = 0, 1. \end{cases}$$

Next, projectors P_s, P_t are defined as follows:

$$P_s[\underline{F}] = \phi_o(s)\ \underline{F}(s_o,t) + \phi_1(s)\ \underline{F}(s_1, t)\ ,$$

$$P_t[\underline{F}] = \psi_o(t)\ \underline{F}(s, t_o) + \psi_1(t)\ \underline{F}(s, t_1)\ .$$

The required function $\underline{U}(s,t)$ is then given, in terms of the Boolean sum $P_s \oplus P_t$ of P_s and P_t by the relation

$$\underline{U}(s,t) = (P_s \oplus P_t)\ [\underline{F}] = P_s[\underline{F}] + P_t[\underline{F}] - P_sP_t[\underline{F}], \qquad (7)$$

where the product projection P_sP_t is defined by

$$P_s P_t[\underline{F}] = \sum_{i=0}^{1} \sum_{j=0}^{1} \phi_i(s)\, \psi_j(t)\, \underline{F}(s_i, t_j) \ . \qquad (8)$$

Whilst the right-hand side of (8) interpolates to $\underline{F}$ at the four vertices of the square $[0, 1] \times [0, 1]$ in the s-t plane, the vector valued function $\underline{U}(s,t)$ given by (7) interpolates to $\underline{F}$ at all points on the boundary of the square. At the same time it maps the points with coordinates (s,t) in the interior of the square onto the nodes with position vector $\underline{U}(s,t)$ in the interior of R. If the parametric representations $\underline{F}(s,t)$ of the arcs AB, BC, CD and DA in the x-y plane are known, then (7) yields the required mapping of the square onto the region R in the form

$$\underline{U}(s,t) = (1-S)\, \underline{F}(0,t) + s\, \underline{F}(1,t) + (1-t)\, \underline{F}(s,0) + t\, \underline{F}(s,1)$$

$$- (1-s)(1-t)\, \underline{F}(0,0) - (1-s)t\, \underline{F}(0,1) - s(1-t)\, \underline{F}(1,0) - st\, \underline{F}(1-1). \qquad (9)$$

3.4. Mesh-Grading Features

3.4.1. The Gordon-Hall Square

In Figure 5 the solid lines divide the Gordon-Hall square into $4n_1n_2$ rectangular subdomains with $N_1 (= 2n_1)$ and $N_2 (=2n_2)$ subdomains along A'B' and A'D', respectively. The centers of these subdomains lie on the dotted lines as shown.

Figure 6 shows a typical subdomain with its center P'_{ij} which has coordinates (s_i, t_j), $0 \leq s_i, t_j \leq 1$, $i=1,2,\ldots, N_1$, $j=1,2,\ldots, N_2$.

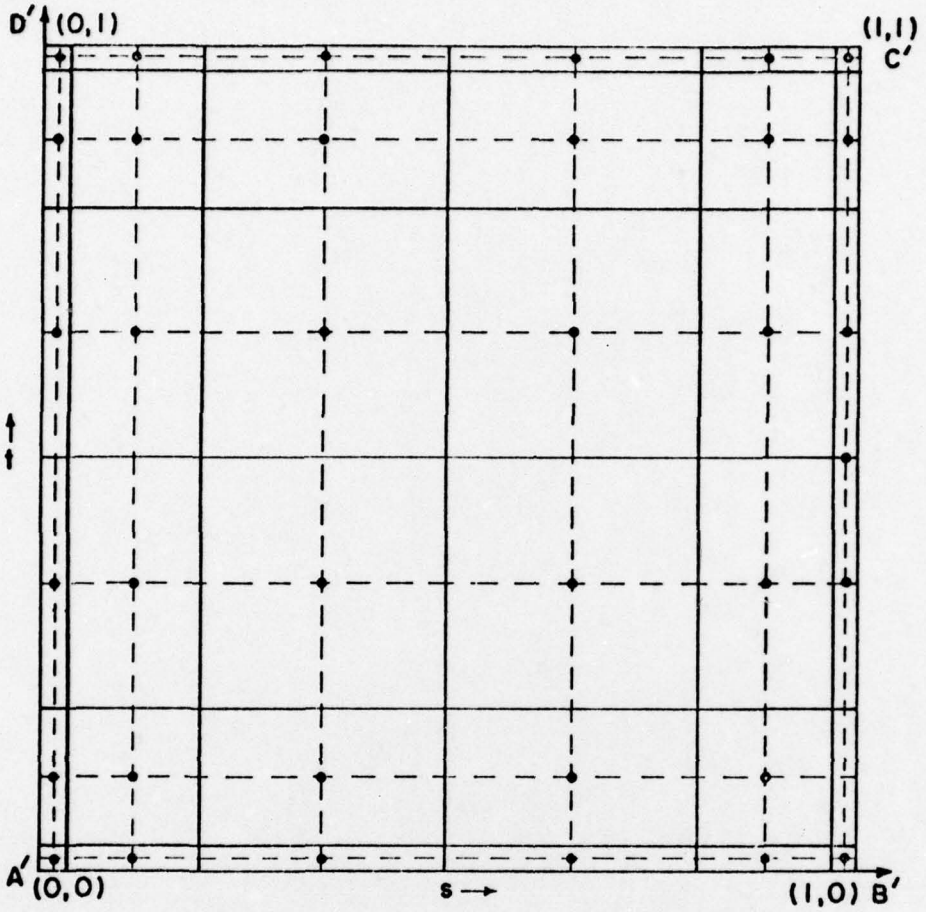

Fig. 5. The pulse version of mesh-grading applied to the Gordon-Hall square.

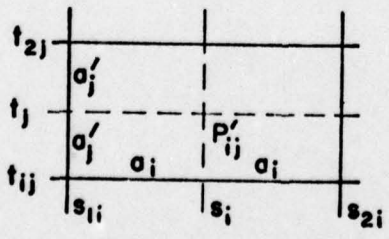

Fig. 6. A typical rectangular subdomain in Figure 5.

The subdomain has sides $2a_i$, $2a'_j$, Figure 6. Using the notation $a_{n_1} = a_{n_1+1} = \Delta_1$; $a'_{n_2} = a'_{n_2+1} = \Delta_2$, we introduce section ratios [20] k_1 and k_2 where $a_1 = a_{N_1} = k_1\Delta_1$; $a'_1 = a'_{N_2} = k_2\Delta_2$, in such a way that the following linear relations hold.

$$a_i = \Delta_1 - \alpha(\frac{N_1}{2} - i), \quad i = 1,2,\ldots,\frac{N_1}{2};$$

$$= \Delta_1 - \beta(i - \frac{N_1}{2} - 1), \; i = \frac{N_1}{2} + 1,\ldots,N_1;$$

where α and β are constants to be determined. Similar relations hold for the a'_j. On expressing α and β in terms of the section ratio k_1, we find that

$$a_i = \Delta_1[1 - \frac{2(1 - k_1)(\frac{N_1}{2} - i)}{N_1 - 2}], \qquad i=1,2,\ldots,\frac{N_1}{2}$$

$$= \Delta_1[1 - \frac{2(1 - k_1)(i - \frac{N_1}{2} - 1)}{N_1 - 2}], \; i = \frac{N_1}{2} + 1,\ldots,N, \tag{10}$$

where the relation $\sum_{i=1}^{n_1} a_i = \frac{1}{4}$ immediately gives

$$\Delta_1 = \frac{1}{(1 + k_1)N_1} .$$

When $k_1 = 1$ (i.e. for the case of a uniform subdivision along the s-axis), we have $\Delta_1 = \frac{1}{2N_1}$, as expected. For the rth interval along the x-axis, the left- and right-end points are, respectively, at

$S_{1r} = \sum_{i=1}^{r-1} 2a_i$ and $S_{2r} = S_{1r} + 2a_r$, when a_r is given by (10). The center of this interval is at $S_r = S_{1r} + a_r$. By applying a similar procedure

to intervals along the t-axis it can be readily verified that we obtain a subdivision of the square in the s-t plane such that:

(i) the coordinates (s_i, t_j) of the center P'_{ij} of the subdomains are given by

$$S_i = \frac{\Delta_1}{N_1 - 2}\,[2i(N_1k_1 - 2 + i - k_1 i) - N_1k_1 + 2],\ i=1,2,..,\frac{N_1}{2}\ ,$$

$$= \frac{1}{2} + \frac{\Delta_1}{2(N_1-2)}\,[(2i-N_1)(3N_1 - N_1k_1 - 4k_1 - 2i - 2ik_1) + 4k_1 - 2N_1],$$

$$i = \frac{N_1}{2} + 1,\ldots,N_1\ , \qquad (11a)$$

i.e.

$$S_i = s_i(N_1, k_1, \Delta_1, i)\ , \quad i = 1,2,\ldots,N_1, \text{ say}, \qquad (11b)$$

and

$$t_j = s_j(N_2, k_2, \Delta_2, j)\ , \quad j = 1,2,\ldots,N_2,$$

where

$$\Delta' = \frac{1}{(1 + k_2)N_2}\ ;$$

(ii) the coordinates of the vertices of the subdomains are (ξ_i, η_j) where

$$\xi_i = \frac{2\Delta_1(i-1)}{N_1 - 2}\,(N_1k_1 - 2 + i - k_1 i),\quad i = 1,2,\ldots,\frac{N_1}{2}$$

$$= \frac{1}{2} + \frac{\Delta_1(2i - N_1 - 2)}{2(N_1 - 2)}\,(3N_1 - N_1k_1 - 4k_1 - 2i + 2ik_1),$$

$$i = \frac{N_1}{2} + 1,\ldots,\ N_1 + 1, \qquad (12a)$$

i.e.

$$\xi_i = \xi_i\,(N_1, k_1, \Delta_1, i),\ i = 1,2,\ldots,N_1 + 1\ , \qquad (12b)$$

with

$$\eta_j = \xi_j\,(N_2, k_2, \Delta_2, j),\ j = 1,2,\ldots,N_2 + 1\ . \qquad (12c)$$

The points P'_{ij} and the vertices (ξ_i, η_j) give rise to images in the x-y plane, under the mapping $\underline{U}$, so that the boundary of the domain R is approximated by a polygon R' whose vertices are the images of the vertices (ξ_i, η_j) which lies on the boundary of the square. This polygon is then effectively divided into quadrilaterals by connecting the image vertices so that the subdomain containing P_{ij} has as vertices the images of the vertices

$$(\xi_i, \eta_j),\ (\xi_{i+1}, \xi_j),\ (\xi_{i+1}, \eta_{j+1}) \text{ and } (\xi_i, \eta_{i+1}),$$

$$i = 1,2,\ldots,N_1;\quad j=1,2,\ldots,N_2.$$

3.4.2. The Zienkiewicz-Phillips Square

Here, since the Gordon-Hall square $[0, 1] \times [0, 1]$ is replaced by the square $[-1, 1] \times [-1, 1]$, which is also subdivided into rectangular domains of the type shown in Figure 6, we have in place of (11) and (12):

(i) The Coordinates (s_i, t_j) of P'_{ij}

$$S_i = -1 + \frac{\Delta_1}{N_1-2}\,[2_i(N_1k_1 - 2 + i - k_1 i) - N_1k_1 + 2],\ i=1,2,\ldots,\frac{N_1}{2}$$

$$= \frac{\Delta_1}{2(N_1-2)}\,[(2i - N_1)(3N_1-N_1k_1-4k_1-2i + 2ik_1) + 4k_1 - 2N_1],$$

$$i = \frac{N_1}{2} + 1,\ldots,\ N_1 \qquad (13a)$$

where

$$\Delta_1 = \frac{2}{(1+k_1)N_1}$$

i.e.

$$s_i = s_i(N_1, k_1, \Delta_1, i) \; ; \tag{13b}$$

$$t_j = s_j(N_2, k_2, \Delta_2, j) \tag{14}$$

where $$\Delta_2 = \frac{2}{(1 + k_2)N_2}$$

(ii) The Coordinates (ξ_i, η_j) of the Vertices of the Subdomains

$$\xi_i = -1 + \frac{2\Delta_1(i-1)}{N_1 - 2}(N_1k_1 - 2 + i - k_1 i), \qquad i=1,2,\ldots, \frac{N_1}{2}$$

$$= \frac{\Delta_1(2i - N_1 - 2)}{2(N_1 - 2)}(3N_1 - N_1k_1 - 4k_1 - 2i + 2ik_1) \; , \tag{15a}$$

$$i = \frac{N_1}{2} + 1, \ldots, N_1+1,$$

or

$$\xi_i = \xi_i(N_1, k_1, \Delta_1, i) \; ; \tag{15b}$$

$$\eta_j = \xi_j(N_2, k_2, \Delta_2, j) \tag{16}$$

By setting k_1 and k_2 to values less than 1, the boundary quadrilateral subdomains can be made much smaller than those near the center of the domain R', so that the charge density can be computed at points very close to the boundary, without the need for the very large values of N_1 and N_2 which would be required with uniform subdivisions.

3.5. Applications of the Automatic Procedures

3.5.1. The Quadrilateral

Consider the quadrilateral ABCD shown in Figure 7. Now

$$\underline{U}(s,t) = x(s,t)\underline{i} + y(s,t)\underline{j}$$

$$= \begin{bmatrix} x(s,t) \\ y(s,t) \end{bmatrix},$$

where $\underline{i}$ and $\underline{j}$ are unit vectors. The four sections of the boundary can be expressed in parameteric form, as indicated in Figure 7, such that we have

$\underline{AB}$: $F(s,t) = F(s,0) = x(s,0)\underline{i} + y(s,0)\underline{j}$,

$$x(s,0) = x_1 + s(x_2 - x_1);\ y(s,0) = y_1 + s(y_2 - y_1);$$

$\underline{BC}$: $\underline{F}(s,t) = \underline{F}(1,t) = x(1,t)\underline{i} + y(1,t)\underline{j}$,

$$x(1,t) = x_2 + t(x_3 - x_2);\ y(1,t) = y_2 + t(y_3 - y_2),$$

with similar expressions for the line segments $\underline{CD}$ and $\underline{DA}$. On applying (9) we have

$$\underline{U}(s,t) = (1-s)\begin{bmatrix} x_1(1-t) + x_4 t \\ y_1(1-t) + y_4 t \end{bmatrix} + s\begin{bmatrix} x_2(1-t) + x_3 t \\ y_2(1-t) + y_3 t \end{bmatrix}$$

$$+ (1-t)\begin{bmatrix} x_1(1-s) + x_2 s \\ y_1(1-s) + y_2 s \end{bmatrix} + t\begin{bmatrix} x_4(1-s) + x_3 s \\ y_4(1-s) + y_3 s \end{bmatrix}$$

$$- (1-s)(1-t)\begin{bmatrix} x_1 \\ y_1 \end{bmatrix} - (1-s)t\begin{bmatrix} x_4 \\ y_4 \end{bmatrix} - s(1-t)\begin{bmatrix} x_2 \\ y_2 \end{bmatrix} - st\begin{bmatrix} x_3 \\ y_3 \end{bmatrix}$$

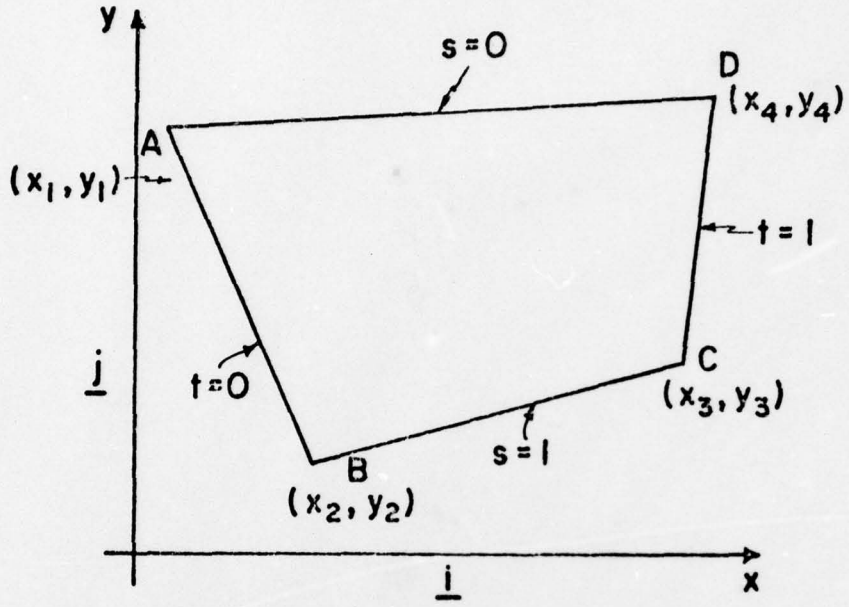

Fig. 7. An image quadrilateral in the x-y plane.

This gives

$$x(s,t) = (1-s)(1-t)x_1 + s(1-t)x_2 + stx_3 + t(1-s)x_4$$

$$y(s,t) = (1-s)(1-t)y_1 + s(1-t)y_2 + sty_3 + t(1-s)y_4 \ . \tag{17}$$

If the quadrilateral is a rectangle with sides AB = a, BC = b, and with its vertices at A(0,0), B(a,0), C(a,b), D(0,b), then (17) becomes

$$x(s,t) = sa, \ y(s,t) = tb \ ,$$

so that the Gordon-Hall mapping reduces to a two-way stretch of the square [0, 1] × [0, 1] parallel to the x- and y-axes.

3.5.2. The triangle

Figure 8 shows a triangle with vertices $A(x_1,y_1)$, $B(x_2,y_2)$, $C(x_3,y_3)$, such that BC is the longest side. Taking ABC as a degenerate quadrilateral $A_1\ B_1\ C_1\ D_1$ with vertices $A_1(x_1', y_1')$, $B_1(x_2', y_2')$, $C_1(x_3', y_3')$, $D_1(x_4', y_4')$, where

$$x_1' = x_1, \quad x_2' = x_2, \ x_3' = \frac{1}{2}(x_2 + x_3), \ x_4' = x_3;$$

$$y_1' = y_1, \ y_2' = y_2, \ y_3' = \frac{1}{2}(y_2 + y_3), \ y_4' = y_3,$$

by introducing a fourth vertex C_1 at the midpoint of BC, (17) gives the required mapping from [0, 1] × [0, 1] onto ABC as

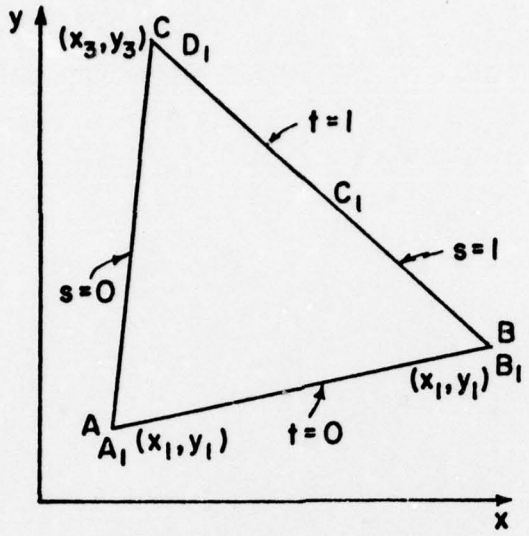

Fig. 8. An image triangle in the x-y plane.

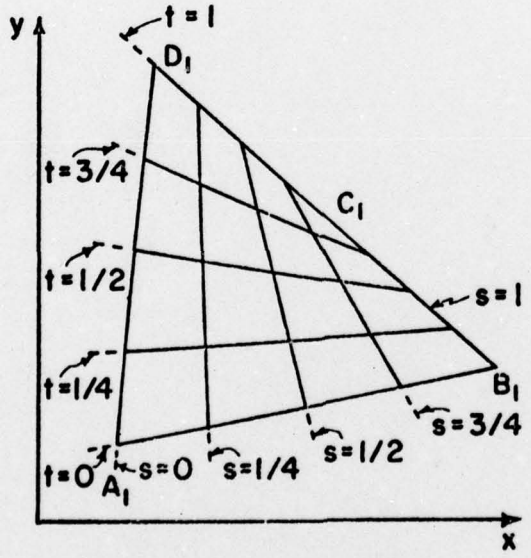

Fig. 9. A subdivision of the triangle in Figure 8.

$$x(s,t) = (1-s)(1-t)x_1 + \frac{1}{2}\,s(2-t)x_2 + \frac{1}{2}\,t(2-s)x_3$$

$$y(s,t) = (1-s)(1-t)y_1 + \frac{1}{2}\,s(2-t)y_2 + \frac{1}{2}\,t(2-s)y_3\ . \qquad (18)$$

An obvious simplification results if A is taken as the origin. In (18) we observe that the parametric lines s = constant and t = constant are mapped onto straight lines in the triangle ABC (Figure 9).

3.5.3. The Ellipse

The points A(a,0), B(0,b), C(-a,0) and D(0,-b), which are the extremities of the axes of the ellipse $b^2x^2 + a^2y^2 = a^2b^2$ (Figure 10), are chosen as the images of the vertices of the Gordon-Hall square. Parametrically, the equation of the ellipse is, for $0 \le s, t \le 1$:

Along AB: $\underline{F}(s,t) = \underline{F}(s,r)$,

$$x = a\cos\frac{s\pi}{2}\ , \quad y = b\sin\frac{s\pi}{2}\ ;$$

Along BC:

$$x = a\cos\frac{\pi}{2}(t+1), \quad y = b\sin\frac{\pi}{2}(t+1);$$

Along CD:

$$x = a\cos\frac{\pi}{2}(s+1), \quad y = -\,b\sin\frac{\pi}{2}(s+1);$$

Along DA:

$$x = a\cos\frac{\pi t}{2}\ , \quad y = -\,b\sin\frac{\pi t}{2}\ .$$

Using (9) we find

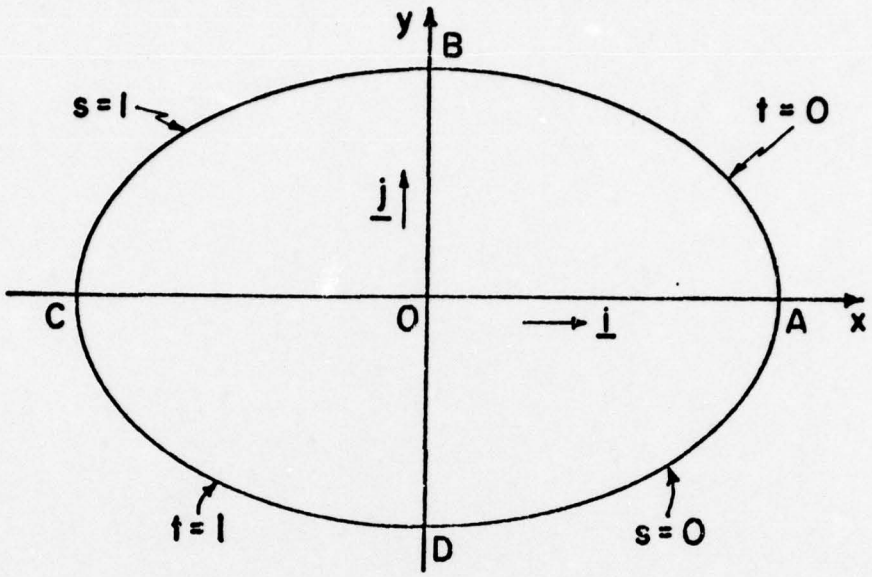

Fig. 10. An ellipse in the x-y plane (showing the parametric description of the boundary).

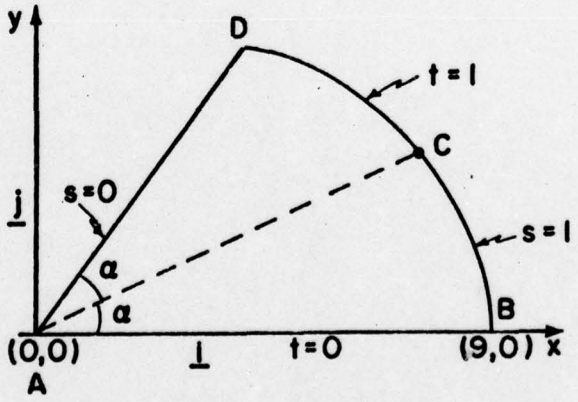

Fig. 11. A sector of an ellipse in the x-y plane.

$$\underline{U}(s,t) = (1-s)\begin{bmatrix} a\cos\frac{\pi t}{2} \\ -b\sin\frac{\pi t}{2} \end{bmatrix} + s\begin{bmatrix} a\cos\frac{\pi}{2}(t+1) \\ b\sin\frac{\pi}{2}(t-1) \end{bmatrix} + (1-t)\begin{bmatrix} a\cos\frac{s\pi}{2} \\ b\sin\frac{s\pi}{2} \end{bmatrix}$$

$$+ t\begin{bmatrix} a\cos\frac{\pi}{2}(s+1) \\ -b\sin\frac{\pi}{2}(s+1) \end{bmatrix} - (1-s)(1-t)\begin{bmatrix} a \\ 0 \end{bmatrix} - (1-s)t\begin{bmatrix} 0 \\ -b \end{bmatrix} - s(1-t)\begin{bmatrix} 0 \\ b \end{bmatrix}$$

$$- st\begin{bmatrix} -a \\ b \end{bmatrix},$$

giving

$$\frac{x}{a}(s,t) = (1-s)\cos\frac{\pi t}{2} - s\sin\frac{\pi t}{2} + (1-t)\cos\frac{\pi s}{2} - t\sin\frac{\pi s}{2} + s+t-1 \tag{19}$$

$$\frac{y}{b}(s,t) = s\cos\frac{\pi t}{2} - (1-s)\sin\frac{\pi t}{2} + (1-t)\sin\frac{\pi s}{2} - t\cos\frac{\pi s}{2} + t-s$$

Here the parametric lines in the s-t plane are mapped, in general, onto curved lines in the x-y plane, unlike for the quadrilateral.

3.5.4. The Ellipse Sector

If the angle of the sector of an ellipse is 2α, we introduce a fourth vertex at the front C($a\cos\alpha$, $b\sin\alpha$), where 2a, 2b are the axes of the ellipse. By defining the parameters s and t for the segments AB, BC, CD and DA of the boundary as shown (Figure 11), and observing that the vector valued function $\underline{F}(s,t)$ assumes the following forms:

$$\underline{AB}: \quad \underline{F}(s,0) = \begin{bmatrix} as \\ 0 \end{bmatrix} ; \quad \underline{BC}: \quad \underline{F}(1,t) = \begin{bmatrix} a \cos(t\alpha) \\ b \sin(t\alpha) \end{bmatrix}$$

$$\underline{CD}: \quad \underline{F}(s,1) = \begin{bmatrix} a \cos(2-s)\alpha \\ b \sin(2-s)\alpha \end{bmatrix} , \quad DA = \underline{F}(0,t) = \begin{bmatrix} at \cos 2\alpha \\ bt \sin 2\alpha \end{bmatrix} ,$$

we obtain

$$\begin{aligned} \frac{x}{a}(s,t) &= s \cos(t\alpha) + t \cos(2-s)\alpha - st \cos\alpha , \\ \frac{y}{b}(s,t) &= s \sin(t\alpha) + t \sin(2-s)\alpha - st \cos\alpha . \end{aligned} \tag{20}$$

3.5.5. The Circle with Two Tangents ('The Circle-With-Tangents')

Figure 12 illustrates a disc bounded partly by a circle of radius a and by the two tangents drawn to it from a point A, the tangents being inclined at an angle α to the x-axis. These tangents meet the circle at B and D, and we take as the 'corner' nodes the points A(a cosec α, 0), B(a sin α, a cos α), C(-a,0), D(a sin α, - a cos α). The parametric forms of the various segments of the boundary are easily seen to be

$$\underline{AB}: \quad \underline{F}(s,0) = a \begin{bmatrix} (\text{cosec}\ \alpha + s(\sin\alpha - \text{cosec}\ \alpha) \\ s \cos\alpha \end{bmatrix}$$

$$\underline{BC}: \quad \underline{F}(1,t) = a \begin{bmatrix} \cos\{(\frac{\pi}{2} - \alpha) + t\ (\frac{\pi}{2} + \alpha)\} \\ \sin\{(\frac{\pi}{2} - \alpha) + t\ (\frac{\pi}{2} + \alpha)\} \end{bmatrix}$$

$$\underline{CD}: \quad \underline{F}(s,1) = a \begin{bmatrix} \cos\{(\frac{\pi}{2} - \alpha) + s\ (\frac{\pi}{2} + \alpha)\} \\ -\sin\{(\frac{\pi}{2} - \alpha) + s\ (\frac{\pi}{2} + \alpha)\} \end{bmatrix}$$

$$\underline{DA}: \quad \underline{F}(0,t) = a \begin{bmatrix} \text{cosec}\ \alpha + t(\sin\alpha - \text{cosec}\ \alpha) \\ - t \cos\alpha \end{bmatrix}$$

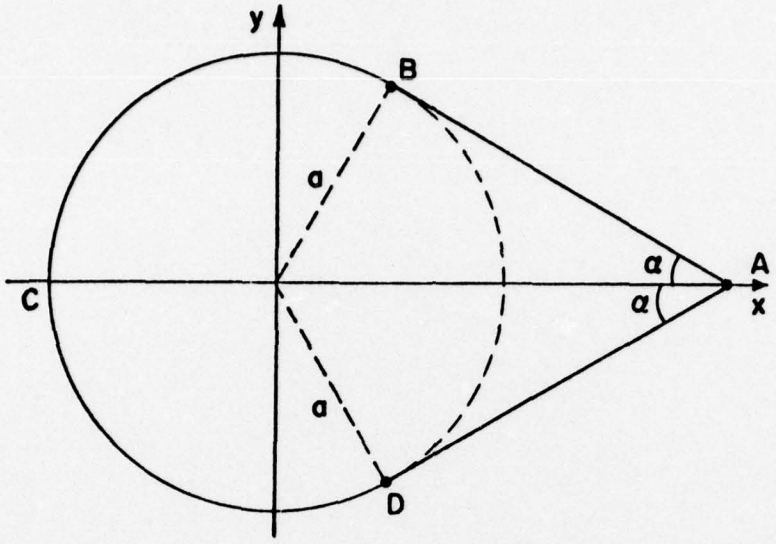

Fig. 12. The 'circle-with-tangents'.

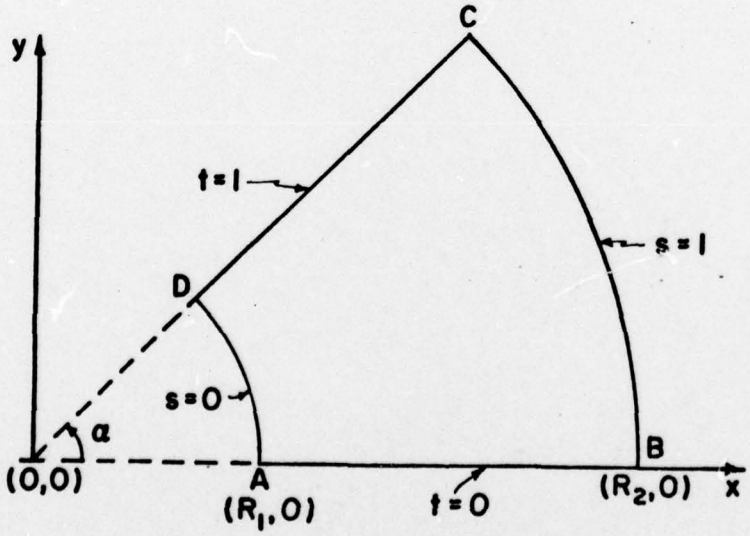

Fig. 13. A sector of an annulus.

From these descriptions, the image $\underline{U}(s,t)$ of the point (s,t) is given by

$$\frac{x}{a}(s,t) = (1-st)\ \mathrm{cosec}\ \alpha + (s+t-2st)(\sin\alpha - \mathrm{cosec}\ \alpha)$$

$$+ s\cos\{(\tfrac{\pi}{2} - \alpha) + t(\tfrac{\pi}{2} + \alpha)\} + t\cos\{(\tfrac{\pi}{2} - \alpha) + s(\tfrac{\pi}{2} + \alpha)\}$$

$$- (s+t-2st)\sin\alpha + st;$$

$$\frac{y}{a}(s,t) = s\sin\{(\tfrac{\pi}{2} - \alpha) + t(\tfrac{\pi}{2} + \alpha)\} - t\sin\{\alpha(\tfrac{\pi}{2} - \alpha) + s(\tfrac{\pi}{2} + \alpha)\}$$

$$+ (s-t)\cos\alpha. \qquad (21)$$

3.5.6. The Annulus Sector

A sector of an annulus is considered here as an example of a non-convex planar domain. Such a sector is shown in Figure 13, the radii being R_1 and R_2 $(R_1 < R_2)$. The parametric equations of the boundary can be written down immediately in the form

$$\underline{F}(s,t) = \begin{bmatrix} \{R_1(1-s) + s\,R_2\}\ \cos\alpha t \\ \{R_1(1-s) + s\,R_2\}\ \cos\alpha t \end{bmatrix}, \qquad (22)$$

where α is the sector angle.

On applying (7) to (22) we find that

$$P_s(\underline{F}) = \underline{F}(s,t), \text{ whilst } P_t(\underline{F}) - P_s P_t(\underline{F}) \equiv \underline{0}.$$

Thus $\underline{U}(s,t)$ is identical to $\underline{F}(s,t)$. The required image in the x-y plane is, therefore, given by

$$x(s,t) = \{R_1(1-s) + s\,R_2\} \cos \alpha t$$

$$y(s,t) = \{R_1(1-s) + s\,R_2\} \sin \alpha t \ . \qquad (23)$$

Gordon and Hall's result for the quarter annulus [6] is easily seen to be a particular case of (23).

Figures 14(i), to 14(vii) show typical subdivision arrangements for the case in which the G-H square is divided uniformly.

3.5.7. Contours Defined by a Set of Points

The application of the Z-P method to a contour defined by four points was given in detail in Sections 3.2.1 and 3.2.2.1. For contours with more than four defining points, which must, therefore, be divided initially into zones (Section 3.2.2.2), the final decomposition is obtained for the first zone by applying the procedure for a single zone. For zone r(r > 1) the process is the same except that in using the four vertices P'_r, P'_{r+1} P'_{n-1}, P'_{n+1-r} defining this zone (Figure 3) the parameters (ξ_s, η_t) given by (6b) are required only for $s=2,3,\ldots,2n_1+1$, $t=1,2,\ldots,2n_2+1$, since the inter-zone nodes corresponding to s=1 have already been accounted for as those corresponding to $s = 2n_1+1$ in zone r-1. Since all the squares are in line, general 'coordinates' (i,j) can be

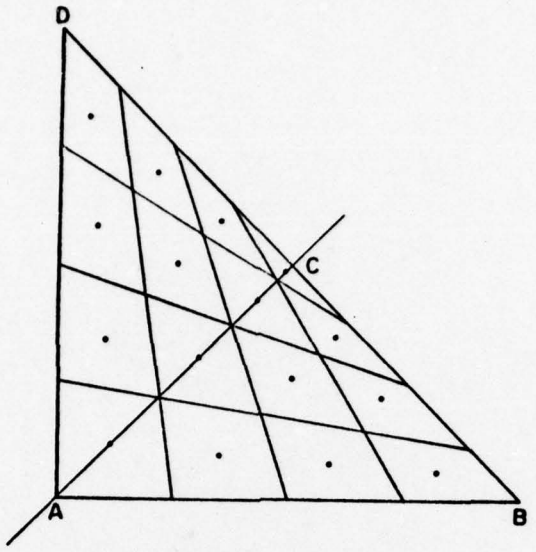

Fig. 14(i). A subdivision scheme for a triangle.

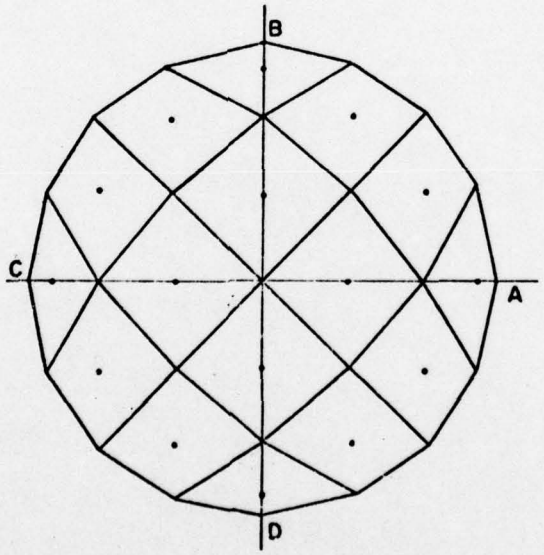

Fig. 14(ii). A subdivision scheme for a circle.

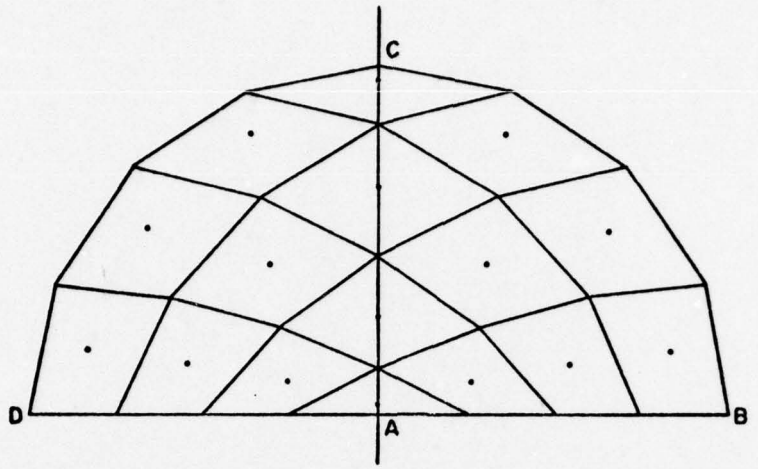

Fig. 14(iii). A subdivision scheme for a semicircle.

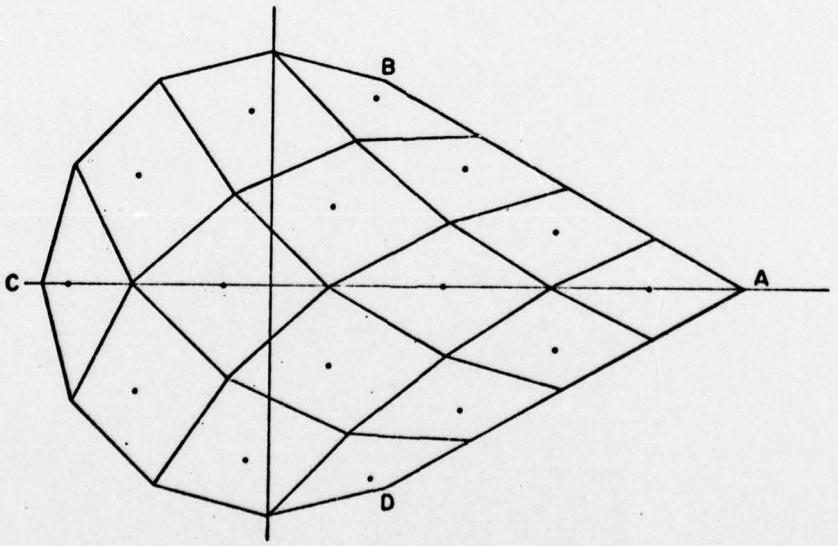

Fig. 14(iv). A subdivision scheme for the 'circle-with-tangents'.

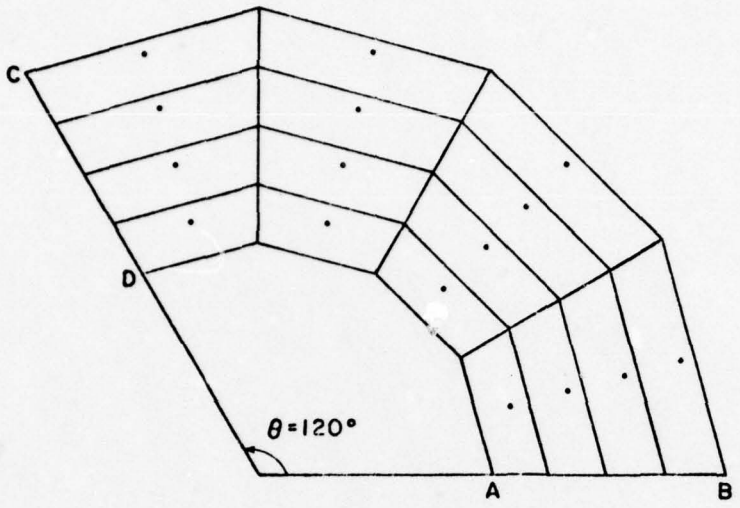

Fig. 14(v). A subdivision scheme for a sector of an annulus.

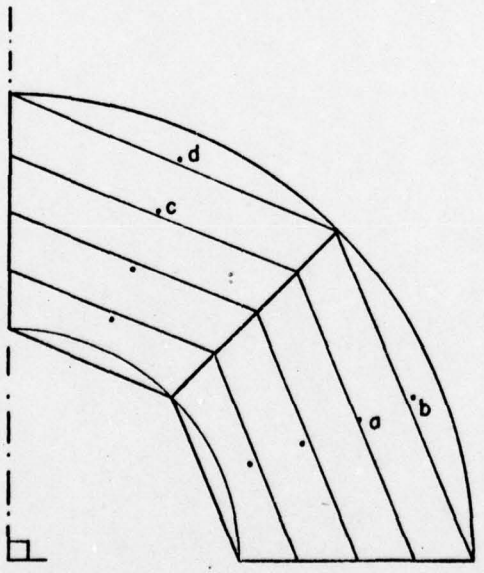

Fig. 14(vi). A sector of an annulus: a subdivision scheme with some matchpoints lying outside their subdomains.

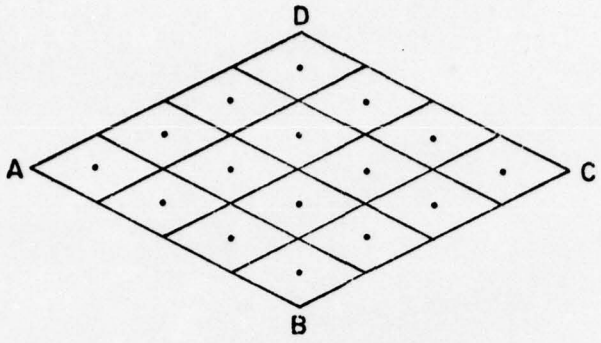

Fig. 14(vii). A subdivision scheme for a diamond.

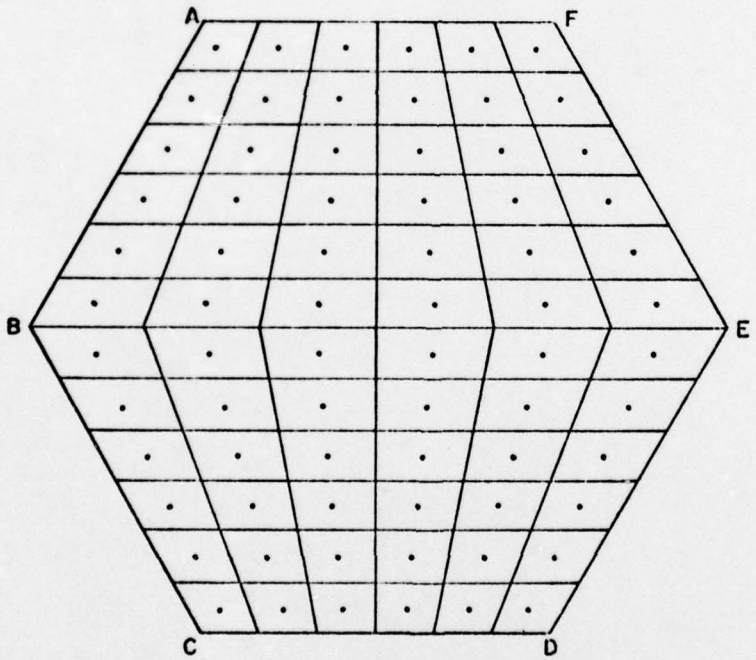

Fig. 14(viii). A subdivision scheme for a regular hexagon.

adopted to identify the vertices for the p zones, where $i=1,2,\ldots 2n_1 p+1$, $j=1,2,\ldots,2n_2+1$.

The layout of the nodes and subdomains generated in a regular hexagon, for $N_1 = 6 = N_2$ and $k_1 = 1.0 = k_2$, are shown in Figure 14(viii).

4. THE INTERACTION MATRIX AND THE POTENTIAL INTEGRAL

4.1. Integration over Triangular and Quadrilateral Domains

The rectangle shown in Figure 6 will be mapped onto a curvilinear quadrilateral subdomain of the disc in the x-y plane (Figure 15) so that the centre P'_{ij} of the rectangle is mapped onto a point P_{ij} within the quadrilateral. This quadrilateral has as vertices the points Q^1_{ij}, Q^2_{ij}, Q^3_{ij}, Q^4_{ij}, which are, respectively the images of the points in the original square with coordinates (ξ_{i+1}, η_j), (ξ_{i+1}, η_{j+1}), (ξ_i, η_{j+1}) and (ξ_i, η_j). For integration purposes the four points in the x-y plane are taken as the vertices of a polygon, so that the disc is ultimately replaced by a collection of such quadrilaterals (Figure 14).

Using the notation of Section 3, Figure 15 may be taken as illustrating the rth subdomain Ω_r of the disc. The four triangular subdomains Ω_{rk}, $k=1,2,\ldots,4$, are those obtained by joining P_{ij} to each of the vertices of the quadrilateral, so that Ω_{rk} has as vertices the points Q^k_{ij}, Q^{k+1}_{ij}, P_{ij}, where $Q^5_{ij} = Q^1_{ij}$. It has been shown that the piecewise integration over Ω_r indicated in (5a) depends on integral expressions of the form C_{srk}. These expressions are best evaluated by the use of the area (or barycentric) coordinates of the triangle Ω_{rk}.

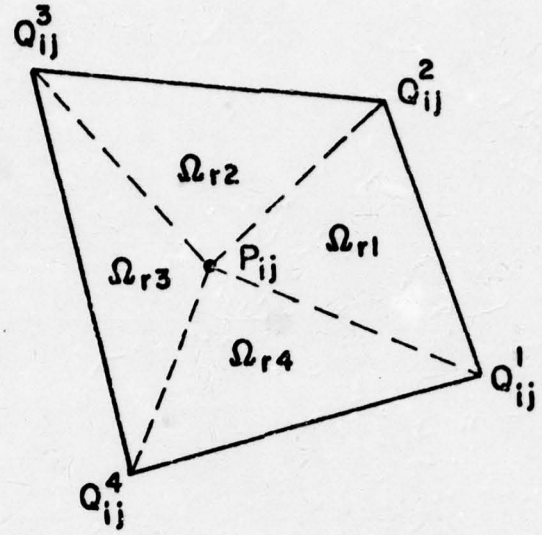

Fig. 15. A quadrilateral subdomain in the x-y plane divided into four triangles.

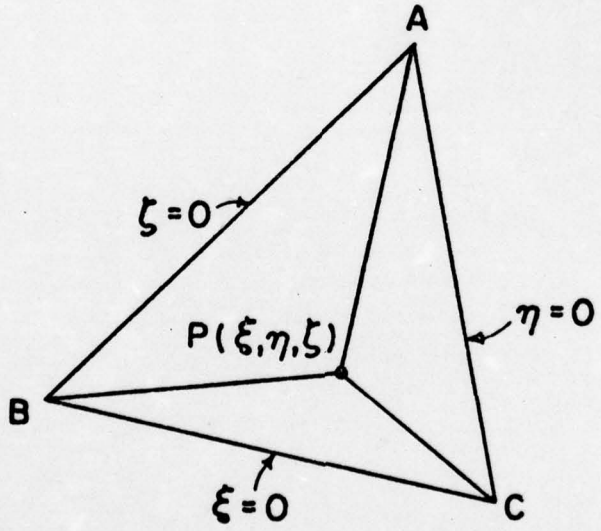

Fig. 16. Area coordinates for the triangle ABC.

The use of these coordinates is a standard procedure in the literature [22-25]. These coordinates are usually denoted by ξ, η, ζ, $0 \leq \xi, \eta, \zeta \leq 1$, and are defined, for any point $P(\xi,\eta,\zeta)$ in the triangle ABC (Figure 16), by

$$\xi = \frac{\Delta_{BPC}}{\Delta_{BAC}} ; \quad \eta = \frac{\Delta_{APC}}{\Delta_{ABC}} ; \quad \zeta = \frac{\Delta_{APB}}{\Delta_{ACB}} ,$$

where Δ_{ABC} is the area of triangle ABC, etc. Thus $\xi + \eta + \zeta = 1$, and the equations of the sides AB, BC and CA can be expressed, respectively, in the forms: $\zeta = 0$, $\xi = 0$, $\eta = 0$.

For any function $f(x,y)$ which is integrable over triangle ABC,

$$\iint_{\Omega_{ABC}} f(x,y)dxdy = 2\,\Delta_{ABC} \int_0^1 \int_0^{1-\eta} f\,\{x(\xi,\eta),\, y(\xi,\eta)\}\, d\xi d\eta, \tag{24a}$$

where Ω_{ABC} denotes the domain of the triangle.

The transformation $\xi' = \frac{\xi}{1-\eta}$, $\eta' = \eta$ converts (24a) to

$$\iint_{\Omega_{ABC}} f(x,y)dxdy = \int_0^1 \int_0^1 (1-\eta')\, f\{\xi(\xi',\, \eta'),\, \eta'\}\; d\xi' d\eta' \tag{24b}$$

This transformation effectively maps the triangle bounded by $\xi = 0$, $\eta = 0$, $\xi + \eta + 1 = 0$ in the ξ-η plane onto the square $[0, 1] \times [0, 1]$ in the ξ'-η' plane.

It is easily shown that if the vertices of the triangle are $A(x_1, y_1)$, $B(x_2, y_2)$, $C(x_3, y_3)$ then

$$\begin{bmatrix} x \\ y \\ 1 \end{bmatrix} = \begin{bmatrix} x_1 & x_2 & x_3 \\ y_1 & y_2 & y_3 \\ 1 & 1 & 1 \end{bmatrix} \begin{bmatrix} \xi \\ \eta \\ \zeta \end{bmatrix} ,$$

i.e.
$$x = a_1\xi + b_1\eta + c_1$$
$$y = a_2\xi + b_2\eta + c_2 \qquad (25)$$

where $a_1 = x_1 - x_3$, $b_1 = y_1 - y_3$, $c_1 = x_3$, etc.

The inverse relation is

$$\begin{bmatrix} \xi \\ \eta \\ \zeta \end{bmatrix} = \frac{1}{2\Delta} \begin{bmatrix} y_2 - y_3 & x_3 - x_2 & x_2y_3 - y_2x_3 \\ y_3 - y_1 & x_1 - x_3 & x_3y_1 - x_1y_3 \\ y_1 - y_2 & x_2 - x_3 & x_1y_2 - y_1x_2 \end{bmatrix} \begin{bmatrix} x_1 \\ y \\ 1 \end{bmatrix} \qquad (26)$$

where $2\Delta = (x_1 - x_3)(y_2 - y_3) - (x_2 - x_3)(y_1 - y_3)$, and $|\Delta|$ is the area of the triangle.

Equation (26) can be expressed in the form

$$\xi = A_1x + B_1y + C_1 \ , \ \eta = A_2x + B_2y + C_2 \ ,$$

$$\zeta = 1 - \xi - \eta,$$

where A_1, B_1, C_1, etc. are constants.

For quadrilaterals of the type shown in Figure 15, uniqueness of the area coordinate representation of points in the various triangles can be ensured across the four interior boundaries by arranging that such lines should correspond to either $\xi = 0$ or $\eta = 0$ in each of the two

triangles in which it belongs. If the coordinates of a typical point in the triangle Ω_{rk} are ξ_k, η_k, ζ_k, then the lines $P_{ij}\,Q'_{ij}$ can be represented as $\eta_1 = 0 = \eta_4$, whilst $P_{ij}\,Q^2_{ij}$ has the representation $\xi_1 = 0 = \xi_2$, etc., as in Figure 17.

4.2. The Potential Due to a Uniform Charge Distribution over a Triangular Domain

The potential at a point (x'_s, y'_s) in the plane of the triangle Ω_{rk}, due to a unit charge density on this triangle is $(4\pi\varepsilon_o)^{-1}\,C_{srk}$, where C_{srk} is given by (5b). On applying the transformation leading to (24b), and dropping the primes on ξ and η, we have (appendix, Section A2.1.1.)

$$C_{srk} = 2\Delta_{rk}\int_0^1 d\eta \int_0^1 \frac{(1-\eta)\,d\xi}{D\{x'_s, y'_s; x(\xi,\eta), y(\xi,\eta)\}} = 2\Delta_{rk}\int_0^1 g(x'_s, y'_s;\eta)d\eta, \quad (27)$$

where Δ_{rk} is the area of Ω_{rk}, and $g(x'_s, y'_s;\eta)$ is given by

$$\alpha_{rk}\, g(x'_s, y'_s;\eta)$$

$$= \log\{a+b\eta + \sqrt{(a+b\eta)^2 + (c+d\eta)^2}\} - \log\{a'+b'\eta + \sqrt{(a'+b'\eta)^2(c+d\eta)^2}\} \quad (28)$$

where $\alpha_{rk} = a^2_{1rk} + a^2_{2rk}$; $a = 1 + R(x'_s, y'_s)$; $b = P-1$;

$c = S(s'_s, y'_s)$; $d = Q$; $a' = R(x'_s, y'_s)$; $b' = P$;

$P = (a_{1rk}b_{1rk} + a_{2rk}b_{2rk})/\alpha^2_{rk}$; $Q = (a_{1rk}b_{2rk} - a_{2rk}b_{1rk})/\alpha^2_{rk}$

$R(x'_s, y'_s) = \{a_{1rk}(c_{1rk} - x'_s) + a_{2rk}(c_{2rk} - y'_s)\}/\alpha^2_{rk}$;

$S(x'_s, y'_s) = \{a_{1rk}(c_{2rk} - y'_s) - a_{2rk}(c_{1rk} - x'_s)\}/\alpha^2_{rk}$.

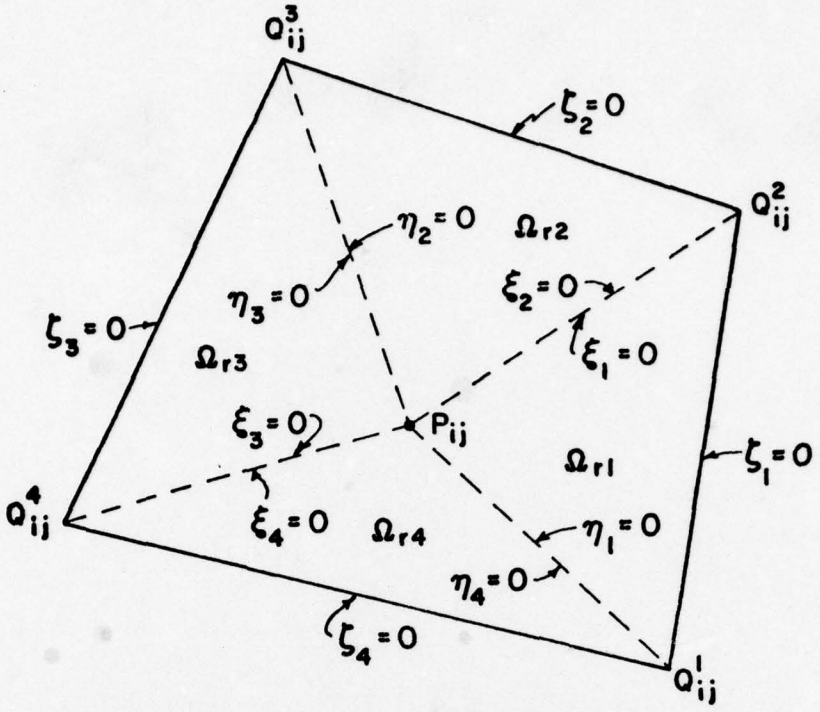

Fig. 17. A quadrilateral subdomain in the x-y plane, with area coordinate representation of interior and exterior boundary lines.

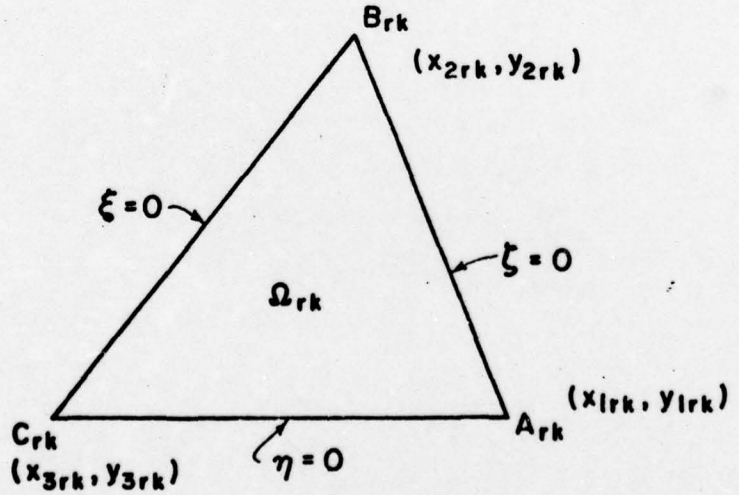

Fig. 18. A triangular subdomain Ω_{rk}.

Here, on referring to Figure 18:

$$a_{1rk} = x_{1rk} - x_{3rk}, \quad b_{1rk} = x_{2rk} - x_{3rk}, \quad c_{1rk} = x_{3rk};$$

$$a_{2rk} = y_{1rk} - y_{3rk}, \quad b_{2rk} = y_{2rk} - y_{3rk}, \quad c_{2rk} = y_{3rk} .$$

The evaluation of the η-integral (Section A2.1.2) gives

$$\left(\frac{\alpha_{rk}}{2\Delta_{rk}}\right) C_{srk} = \bar{E}(1) + \bar{E}'(0) - \bar{E}(0) - \bar{E}'(1) ,$$

where $\bar{E}(\eta) = E(a,b;\eta), \quad \bar{E}'(\eta) = E(a', b';\eta)$,

and $$E(a,b;\eta) = \frac{c + d\eta}{d} \log \{a+b\eta + \sqrt{(a+b\eta)^2 + (c+d\eta)^2}\}$$

$$- \frac{ad - bc}{d\sqrt{b^2 + d^2}} \log \frac{d\{a+b\eta+ \sqrt{(a+b\eta)^2+(c+d\eta)^2}\}- (c+d\eta)(b+ \sqrt{b^2+d^2})}{d\{ a+b\eta+ \sqrt{(a+b\eta)^2+(c+d\eta)^2}\} - (c+d\eta)(b- \sqrt{b^2+d^2})}$$

An alternative expression for C_{srk}, which is less susceptible to round-off errors is (Section A2.1.2)

$$\left(\frac{\alpha_{rk}}{2\Delta_{rk}}\right) C_{srk} = \bar{F}(1) + \bar{F}'(0) - \bar{F}(0) - \bar{F}'(1) , \tag{29}$$

where $\bar{F}(\eta) = F(a,b;\eta), \quad \bar{F}'(\eta) = F(a',b';\eta)$,

and $$F(a,b;\eta) = \frac{c+d\eta}{d} \log \{a+b\eta + \sqrt{(a+b\eta)^2 + (c+d\eta)^2}\}$$

$$+ \frac{ad - bc}{d\sqrt{b^2+d^2}} \log [(b^2+d^2)\eta + ab+cd + \sqrt{\{(b^2+d^2)\eta+ab+cd\}^2+(ad-bc)^2}]$$

For an arbitrary field point with coordinates (x_s', y_s', z_s'), which need not lie in the plane of the triangle, the distance function D in (27) is replaced by

$$\bar{D}\ \{x_s', y_s', z_s';\ x(\xi,\eta), y(\xi,\eta)\} = \{(x-x_s')^2 + (y-y_s')^2 + z_s'^2\}^{1/2}\ .$$

In place of (28) we now have (Section A2.2.1)

$$\alpha_{rk}\ g(x_s', y_s', z_s';\eta)$$

$$= \log\ \{a+b\eta + \sqrt{(a+b\eta)^2+(c+d\eta)^2+e^2}\} - \log\{a'+b'\eta+ \sqrt{(a'+b'\eta)^2+c+d\eta)^2+e^2}\},$$

where $e = z_s'/\alpha_{rk}$, and the other constants are as for (28). On evaluating the η-integral (Section A2.2.2) we find that

$$\alpha_{rk} \int_0^1 g(x_s', y_s', z_s';\eta)d\eta = \bar{G}(1) + \bar{G}'(0) - \bar{G}(0) - \bar{G}'(1),$$

where $\bar{G}(\eta) = G(a,b;\eta)$, $\bar{G}'(\eta) = G(a',b';\eta)$,

and $$G(a,b;\eta) = \frac{c+d\eta}{d} \log\ \{a+b\eta + \sqrt{(a+b\eta)^2 + (c+d\eta)^2 + e^2}\}$$

$$+ \frac{ad - bc}{d\sqrt{b^2+d^2}} \log\ [(b^2+d^2)\eta + ab+cd+\sqrt{\{(b^2+d^2)\eta+ab+cd\}^2+(ad-bc)^2+e^2(b^2+d^2)}]$$

$$+ \frac{e}{d} \sin^{-1}\left[\frac{de\sqrt{(a+b\eta)^2 + (c+d\eta)^2 + e^2}}{\sqrt{\{(c+d\eta)^2+e^2\}\ \{ad-bc)^2+e^2(b^2+d^2)\}}}\right] .$$

Thus the potential at an arbitrary point in space, due to a unit charge density on the triangle Ω_{rk} is $(4\pi\varepsilon_o)C_{srk}$, where

$$\left(\frac{\alpha_{rk}}{2\Delta_{rk}}\right) C_{srk} = \bar{G}(1) + \bar{G}'(0) - \bar{G}(0) - \bar{G}'(1) \quad . \tag{30}$$

This expression for C_{srk} reduces, as expected, to (29) when e = 0.

Expressions of the form $\log [X + \sqrt{X^2 + Y^2}]$ occur in both (29) and (30). If X is negative such expressions are best computed by using the alternative form

$$\log\left[\frac{Y^2}{-X + \sqrt{X^2 + Y^2}}\right] .$$

5. RESULTS AND OBSERVATIONS

5.1. Charge Distribution

The charge density on an ellipse with semiaxes a and b is [21]

$$\sigma' = \frac{Q}{4\pi ab}\left(1 - \frac{x^2}{a^2} - \frac{y^2}{b^2}\right)^{-1/2} , \tag{31}$$

where (x,y) are the coordinates of a typical point in the ellipse, and Q is the total charge. If an elliptical disc is maintained at unit potential, then observing that the charge accumulates on both sides of the disc, (31) gives the charge distribution σ on the disc as

$$\sigma = \frac{C}{2\pi ab}\left(1 - \frac{x^2}{a^2} - \frac{y^2}{b^2}\right)^{-1/2} , \tag{32}$$

where C is the capacitance of the disc as given in the appendix (Section A.1.).

The exact charge distribution (32) has been compared with the computed values for a circle of radius/cm (Figure 19), and for an ellipse with a = 5 cm, b = 1 cm (Figure 20). The results show that for a given number of subdivisions of the ellipse or circle (i.e. for fixed values of N_1 and N_2 as defined for the Gordon-Hall square) the use of non-uniform section ratios k_1 and k_2 gives a charge distribution which is more accurate than for uniform section ratios. As expected, a non-uniform section ratio allows charge densities to be computed very near the edges, and the approach to the square root singularity at the edges is more clearly brought out. For $N_1 = 8 = N_2$ for example, at comparable points in a circular disc, working with uniform section ratios (i.e. $k_1 = 1.0 = k_2$) results in error margins of 24% near the edges and 1.7% near the center, whereas for $k_1 = 0.1 = k_2$ the error margins are 4% and 0.7%. For an elliptical disc with a = 5 cm, b = 1 cm, the figures are 52% and 1.4% for unity section ratios, and 4% and 0.8% for section ratios of 0.1.

The distribution for unity section ratios for a square of edge 2 cm (Figure 21) agrees with Harrington's result [3] to within 1% everywhere except at the node nearest to the edge where the difference is 1.7% (Figure 21). The beneficial effect of non-uniform section ratios is again evident. In Figure 22, drawn for a regular hexagon of side 1 cm, the distribution shows the expected symmetry and the rise in the charge density as one approaches the edges.

Figure 23 compares the computed charge distribution over a semicircle with that for a full circle. A similar figure (Fig. 24)

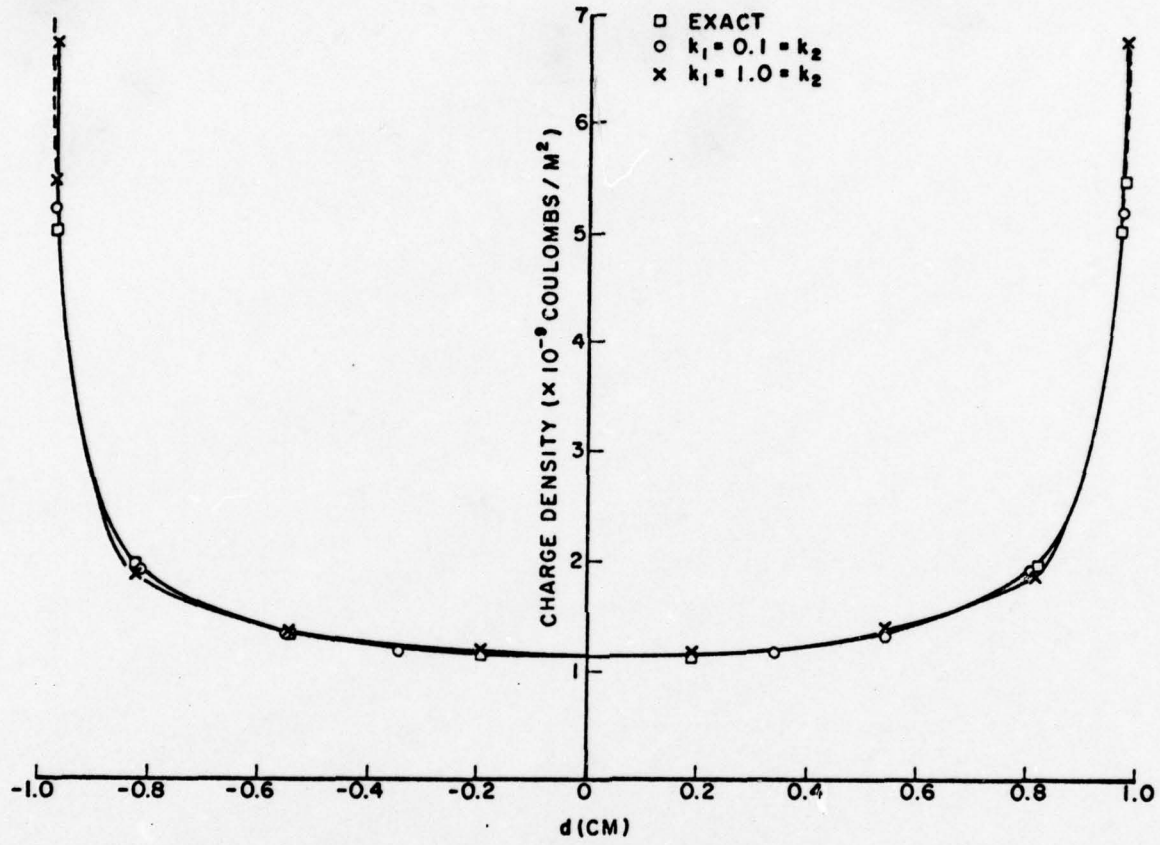

Fig. 19. The circle: radius = 1 cm. Charge distribution.

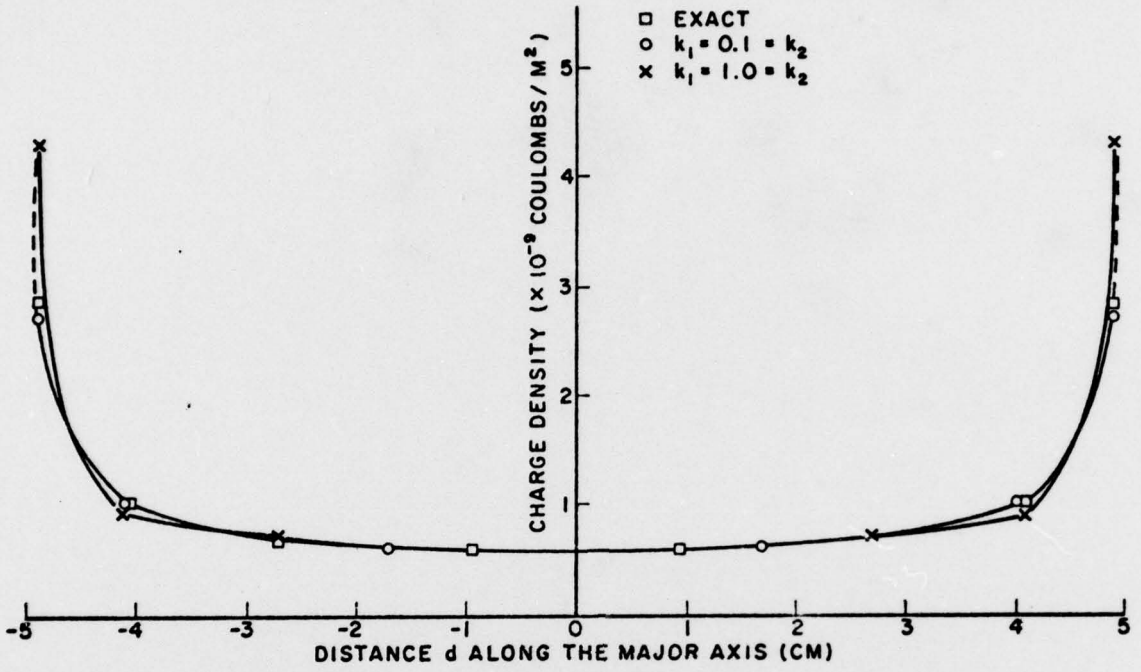

Fig. 20. The ellipse: a = 5 cm, b = 1 cm. Charge distribution.

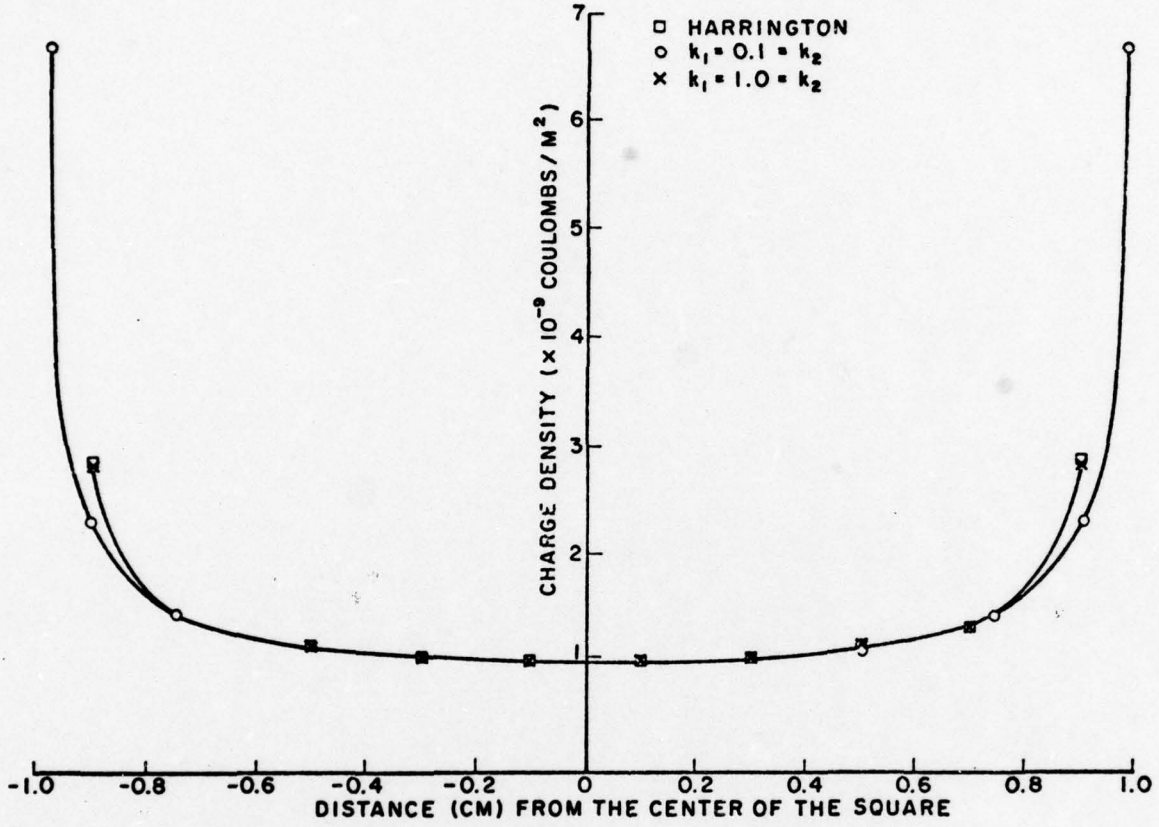

Fig. 21. The square: 2 cm × 2 cm. Charge distribution.

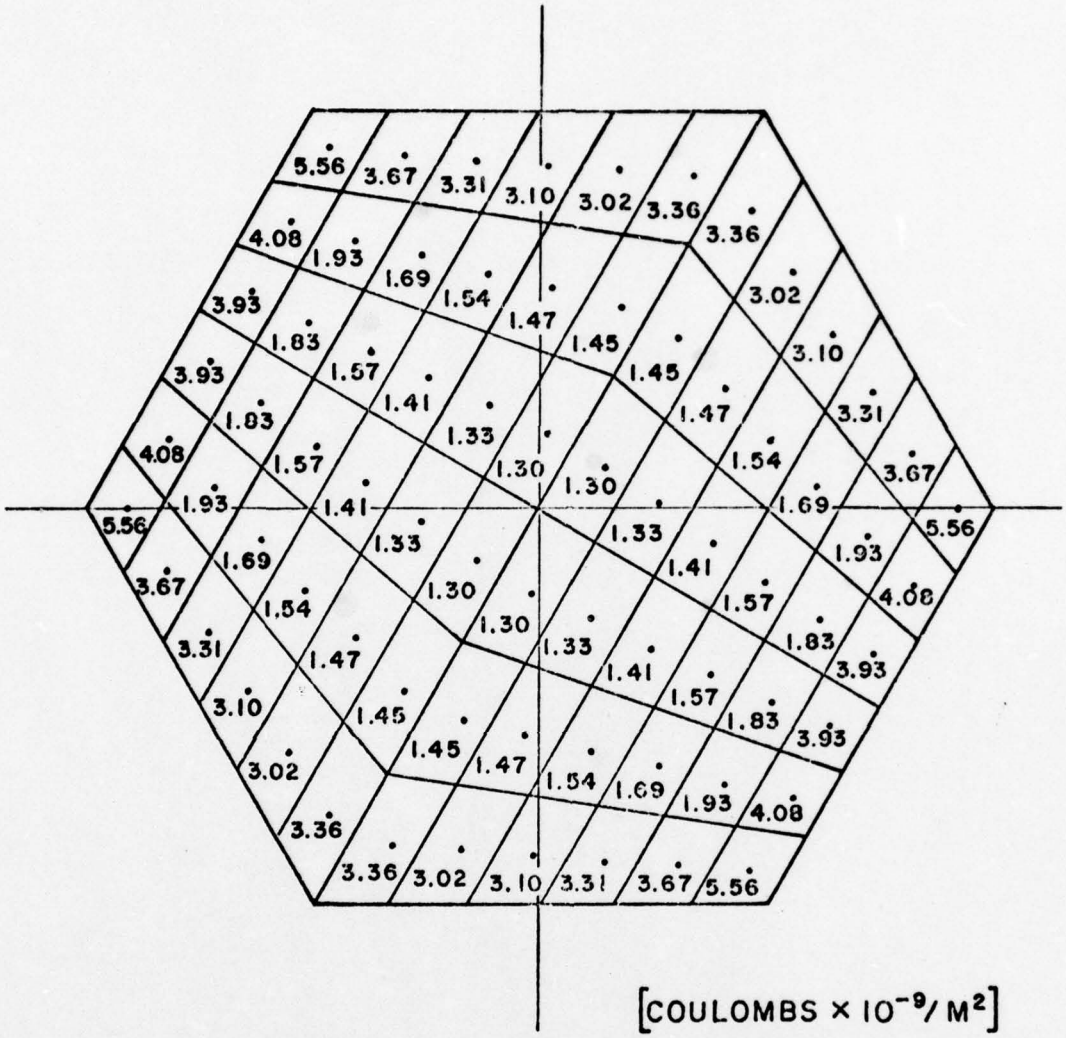

Fig. 22. The regular hexagon: side 1 cm, $N_1 = 6 = N_2$, $k_1 = 1.0 = k_2$. Charge distribution.

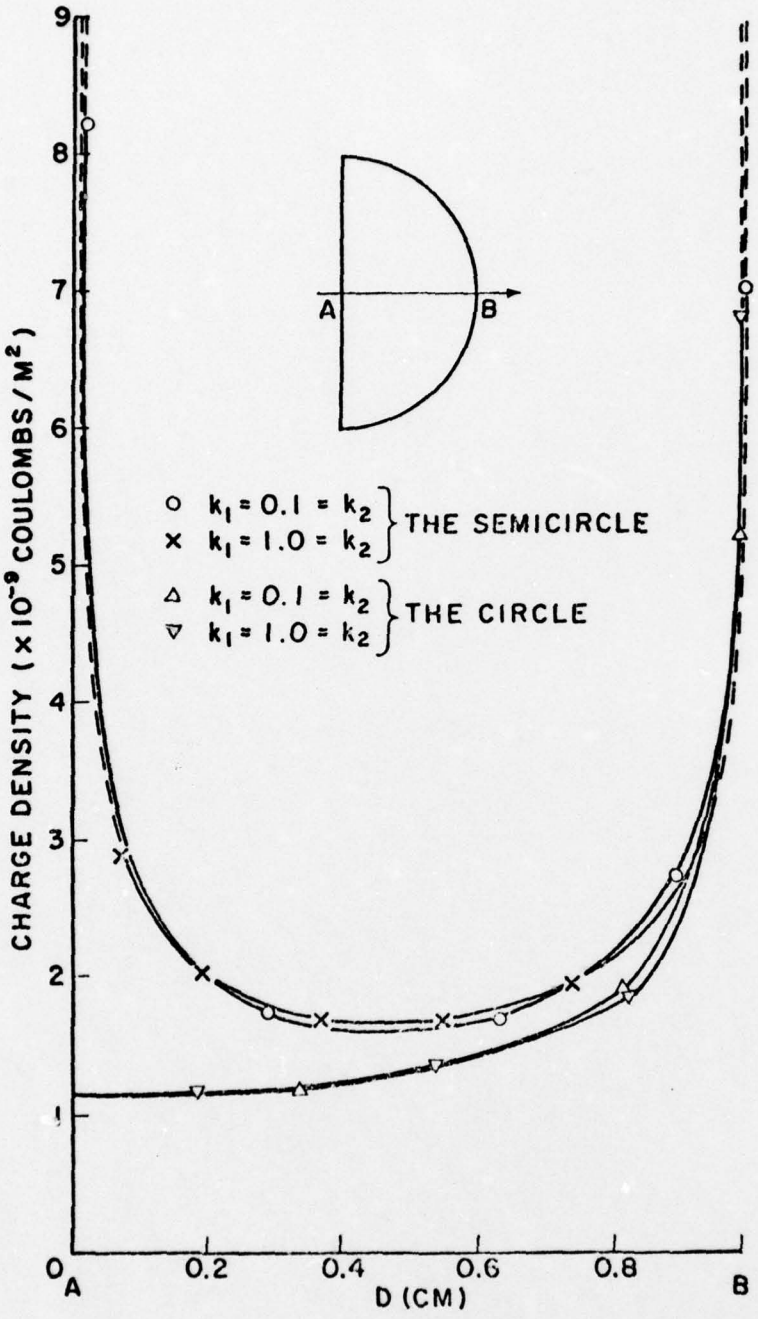

Fig. 23. The circle and semicircle: radius = 1 cm. Charge distribution.

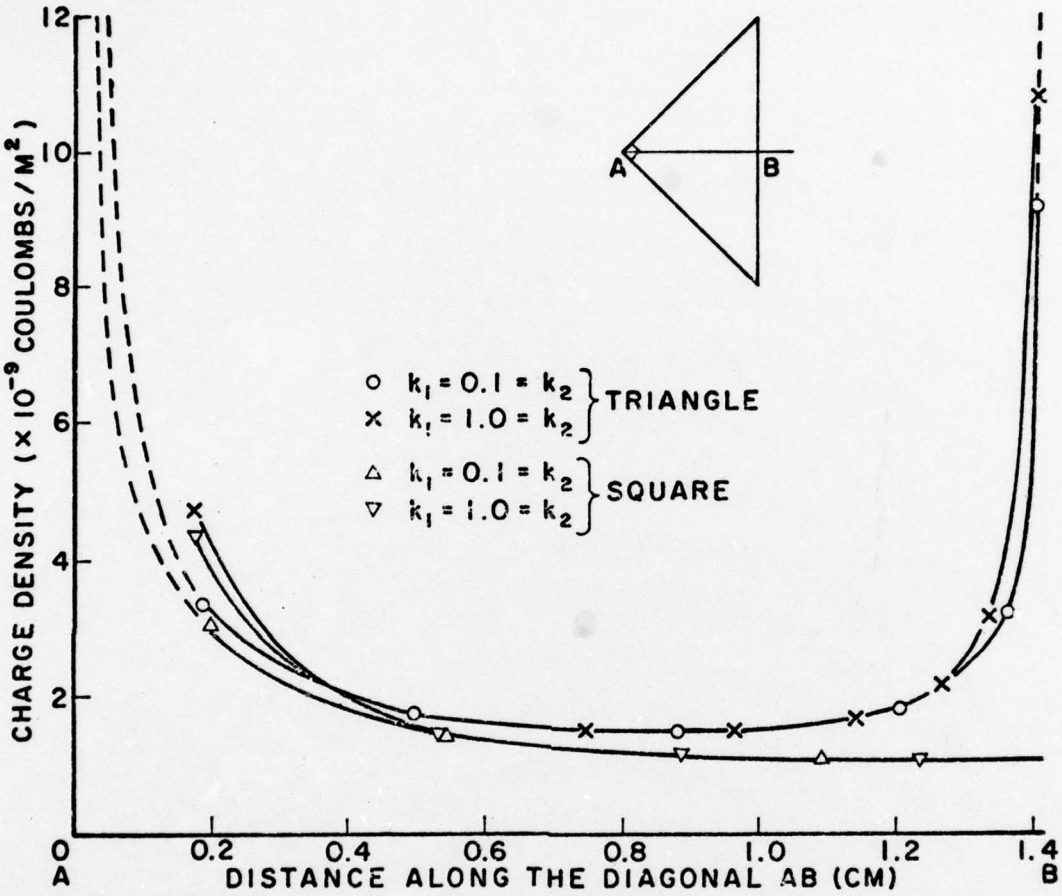

Fig. 24. The triangle and the square: side of square 2 cm. $N_1 = 8 = N_2$. Charge distribution.

has been drawn for a square and a triangular half of this square.

5.2. Capacitance

It is shown in the appendix that the capacitance of an elliptical disc with semi-major axis a is

$$C = 4\pi a\varepsilon_o / K(e) \ , \tag{33}$$

where K is the complete elliptic integral of the first kind and the modulus e is the eccentricity of the ellipse. A computer program (PROGAE) computes C from this expression, using the Hastings approximation [17,28] for K(k) in the form

$$K(k) = \sum_{r=0}^{4} a_r \bar{k}^{2r} - 2\left[\sum_{r=0}^{4} b_r \bar{k}^{2r}\right] \log \bar{k} + \varepsilon(k),$$

where

$$|\varepsilon(k)| \leq 2 \times 10^{-8}, \quad \bar{k}^2 = 1 - k^2 \ , \quad \text{and}$$

$$a_0 = 1.38629436112 \qquad b_0 = 0.5$$

$$a_1 = 0.09666344259 \qquad b_1 = 0.12498593597$$

$$a_2 = 0.03590092383 \qquad b_2 = 0.06880248576$$

$$a_3 = 0.03742563713 \qquad b_3 = 0.03328355346$$

$$a_4 = 0.01451196212 \qquad b_4 = 0.00441787012$$

For a circle of radius a we use the well-known result $C = 8a\varepsilon_o$, which, as shown in Section A.1, is a particular case of (33).

Convergence curves which show the variation of C with $(N_1 N_2)^{-1}$ for the circle and the square (Figure 25) indicate that section ratios

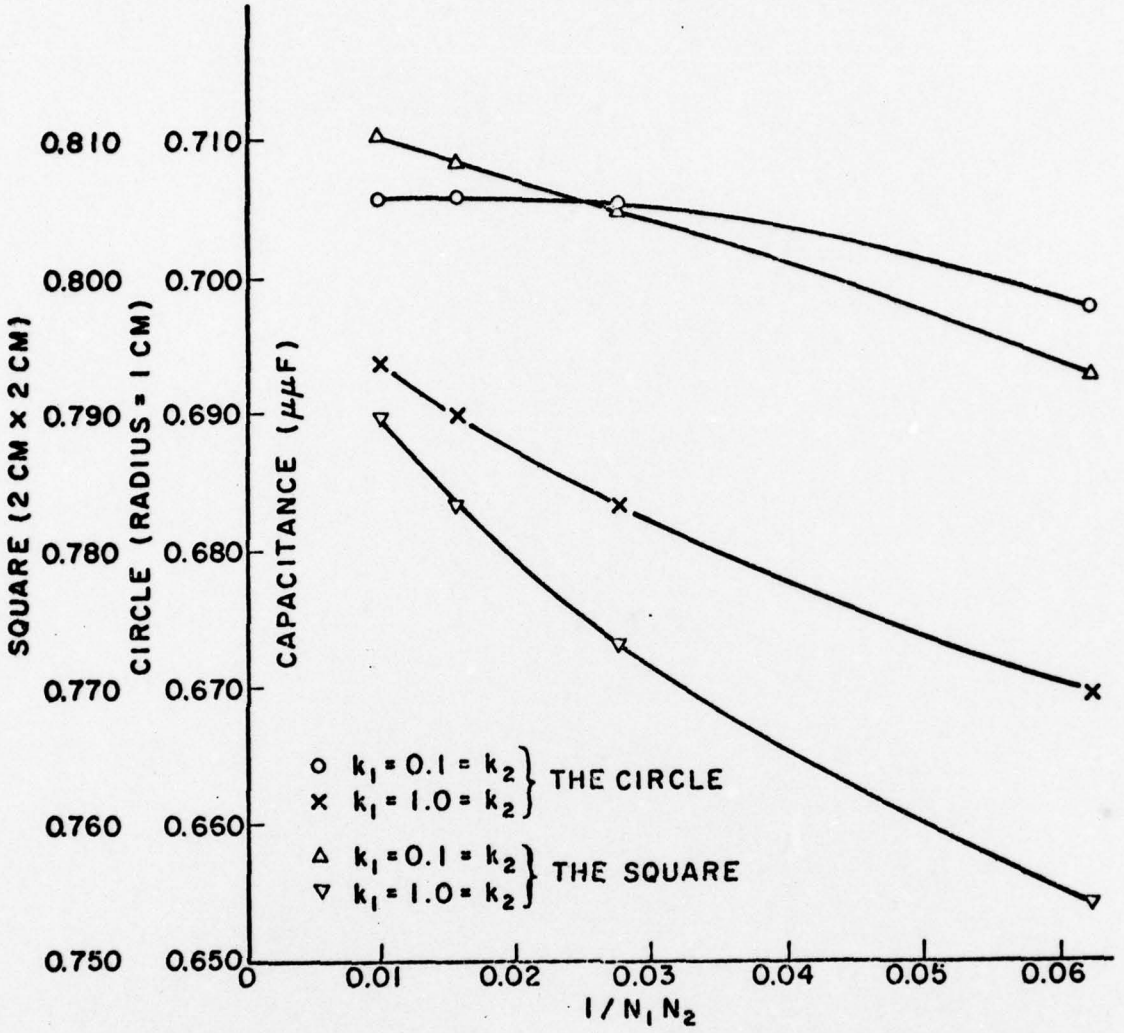

Fig. 25. Capacitance vs. $1/N_1N_2$. The circle (R = 1 cm), the square (2 cm × 2 cm).

of 0.1 give a more accurate value for the capacitance than unity section ratios. The greater accuracy obtained with section ratios less than unity, which was observed for the charge density, is also reflected in all the capacitance computations. This improvement in accuracy agrees with similar observations made in the investigation of current distribution effects in perfectly-conducting cylinders [20].

To estimate the capacitance for an infinite number of subdivisions (i.e. the asymptotic capacitance) we use a power series procedure which gives C as

$$C = \sum_{i=0}^{\infty} \frac{\bar{C}_i}{(N_1 N_2)^i} \tag{34}$$

If there are m sets of computed data in the form $\{N_{1s}, N_{2s}; C_s\}$, $s = 1,2,\ldots,m$, then by truncating (34) in the form

$$C = \sum_{i=0}^{m-1} \frac{\bar{C}_i}{(N_1 N_2)^i} ,$$

the following matrix equation

$$\left[\frac{1}{(N_{1s} N_{2s})^{r-1}}\right] [\bar{C}_{r-1}] = [C_s] ,$$

$r = 1,2,\ldots, m; \quad s = 1,2,\ldots, m,$

is then solved to give $\bar{C}_o$ as an estimate of the asymptotic capacitance.

For the circle, the asymptotic capacitance computed for various sets of data corresponding to Figure 25 are given in Table 1. The

deviations of the values for section ratios of 1.0 and 0.1 are, respectively, within 0.9% and 0.2% of the exact value. The capacitance for $N_1 = 10 = N_2$ (i.e. for the largest values of N_1 and N_2 used) is found to differ from the exact value by 0.37%, whereas for $N_1 = 8 = N_2$ and for the same section ratios, the error is slightly less (0.31%). This gives an indication of the effect of the increase of round-off with the number of subareas.

Since an inscribed polygon underestimates the area of any convex domain, one would expect the computed capacitance for such domains to be lower than the exact value. This is found to be the case for the circle and for the other convex domains investigated. Tables 2, 9 and 12 list the computed values of capacitance for the ellipse, the semicircle and the 'circle-with-tangents' and also give the percentage deviation of the area of the inscribed polygon (computed by adding the areas of all the triangular subdomains) from the area of the original domain.

For polygonal discs on the other hand, the mesh generation procedures ensure that the inscribed polygon is the same as the original domain, Figs. 14(i), 14(vii) and 14(viii), so that the area of the inscribed polygon as computed agrees with the area of the original domain up to the fifth significant figure at least (see Tables 4-7 for the regular hexagon, the diamond, the rectangle and the triangle). Computations for the square of edge 2 cm (Figure 25 and Table 3) show that the capacitance for $N_1 = 10 = N_2$ and section ratios of 0.1 (i.e. 0.8102 $\mu\mu$ F) is within 0.43% of the asymptotic

value (0.8137 μμ F). The asymptotic value obtained by Table 4 is 0.34 e.s.u. which is 0.8156 μμ F. For the diamond (Table 5a) and the rectangle with dimensions 3.3 cm × 1.4 cm (Table 6), the capacitance computed for $N_1 = 8 = N_2$ and 0.1 section ratios are, respectively, 0.6510 μμ F and 0.9029 μμ F. De Meulenaere and Van Bladel [29] give 0.661 μμ F and 0.897 μμ F.

The results for the sector of an annulus (the only non-convex domain investigated here) indicate that care must be taken in approximating domains by polygons. It is important to ensure that the match point generated lies not only within the curvilinear quadrilateral corresponding to it, but also within the final quadrilateral obtained when the curved sides are replaced by straight lines. When the sector angle is 180° and the section ratios are unity, this condition holds when $N_1 = 8 = N_2$, but it is violated when $N_1 = 4 = N_2$ (Figure 14(vi)). A low section ratio can also give a match point lying outside its quadrilateral. Thus, for example, for $\theta = 180°$ and $N_1 = 8 = N_2$ (Table 10) a section ratio of 0.1 produces this anomaly, as also happens when $\theta = 120°$ and $N_1 = 4 = N_2$. Match points are, however, properly situated in the latter case when the section ratios are unity.

Generally a violation of the match point condition at certain points leads to a distortion of the charge distribution, including the existence of negative charge distributions at some of these points. It also gives for the approximating polygon an area which is larger than that of the original domain mainly because of the resulting

duplication of triangular subdomains as the area is computed. As a guide, well-positioned match points can be ensured by choosing N_1 and N_2 in proportion to the lengths of the corresponding arcs of the domain boundary.

The effect of the distortion in the shapes of the quadrilaterals, when the match point condition is met, has been investigated by computing the percentage errors in the values obtained for the area and the capacitance for ellipses with aspect ratios (i.e. minor axis/major axis) from 1 to 0.2 (Table 11). The results show, for the coarse subdivision used ($N_1 = 4 = N_2$), that the area is in error by 2.6% in all cases. The corresponding figure for the capacitance varies from 5.4% for an aspect ratio of 1 to 4.9% when this ratio is 0.2. These errors are thus due more to the coarseness of the subdivision than to the shapes of the quadrilateral subdomains.

The computations also show that the capacitance of half of a disc is greater than half the capacitance of the complete disc.

6. CONCLUSION

A method of moments technique of solving the singular integral equation satisfied by the charge distribution on perfectly-conducting flat plates of arbitrary shape, which uses automatic mesh generation techniques, has been presented. The method relies on the use of graded quadrilateral subdomains and has been applied to a variety of disc shapes, including the rectangle for which the quadrilateral subdomains reduce to rectangles. The procedure yields charge distributions and values of

capacitance which are in excellent agreement with the exact values for the circle and the ellipse, as well as with published numerical results for the rectangle obtained by other methods of computation. The results indicate that with a moderate number of subdomains it is possible to obtain values of capacitance which are accurate to within 0.5%.

Table 1:
The Circle
Radius = 1 cm: Capacitance

Exact Value of Capacitance: 0.70800 μμF

$N_1 = N_2 = N$	$k_1 = k_2 = k$	Asymptotic Capacitance	
		Computed Value (μμF)	% Error
6, 8, 10	1.0	0.7017	0.89
6, 8, 10	0.1	0.7035	0.65
6, 8	0.1	0.7065	0.21

Table 2:
The Ellipse
Semi Axes: 5 cm, 1 cm: Capacitance

N	k	Area		Capacitance	
		Computed $x10^{-2}$ m^2	% Error	Computed Value (μμF)	% Error
4	1.0	0.15307	2.6	1.753	4.9
4	0.1	0.15450	1.6	1.817	1.5
8	1.0	0.15607	0.64	1.802	2.3
8	0.1	0.15495	1.4	1.838	0.29

Asymptotic Capacitance

N	k	Computed Value (μμF)	% Error
4, 8	1.0	1.818	1.4
4, 8	0.1	1.846	0.11

Table 3:
The Square
Edge = 2 cm

N	k	Asymptotic Capacitance (μμF)
4, 6, 8	1.0	0.7988
4, 6, 8, 10	1.0	0.8037
4, 6, 8	0.1	0.8126
4, 6, 8, 10	0.1	0.8137

Table 4:
The Regular Hexagon
Edge = 1 cm

Exact Area: $0.25980 \times 10^{-3} m^2$

N	k	Area ($\times 10^{-3} m^2$)	Capacitance (μμF)
4	1.0	0.25980	0.6120
4	0.1	0.25980	0.6345
6	1.0	0.25980	0.6234
6	0.1	0.25980	0.6415

Asymptotic Capacitance

N	k	Computed Value (μμF)
4, 6	1.0	0.6325
4, 6	0.1	0.6471

Table 5:
The Diamond

(a) Semi Axes: a = 1.65 cm, b = 0.7 cm

Exact Area: $0.231 \times 10^{-3} m^2$

N	k	Area ($\times 10^{-3} m^2$)	Capacitance ($\mu\mu F$)
4	1.0	0.23100	0.6063
4	0.1	0.23100	0.6380
8	1.0	0.23100	0.6305
8	0.1	0.23100	0.6510

(b) Semi Axes: a = 2 cm, b = 1 cm

Exact Area: $0.10000 \times 10^{-3} m^2$

N	k	Area ($\times 10^{-3} m^2$)	Capacitance ($\mu\mu F$)
4	1.0	0.10000	0.3914
4	0.1	0.10000	0.4117

Table 6:
The Rectangle: 3.3 cm x 1.4 cm

Exact Area: $0.46200 \times 10^{-3} m^2$

N	k	Area ($\times 10^{-3} m^2$)	Capacitance ($\mu\mu F$)
8	1.0	0.46200	0.8755
8	0.1	0.46200	0.9029

Table 7
The Triangle
Adjacent Sides: 2 cm, 1 cm; Included Angle: 90°
Exact Area: $0.20000 \times 10^{-3} m^2$

N	k	Area ($\times 10^{-3} m^2$)	Capacitance (μμF)
4	1.0	0.20000	0.5648
4	0.1	0.20000	0.5958
6	1.0	0.20000	0.5800
6	0.1	0.20000	0.6050
8	1.0	0.20000	0.5879
8	0.1	0.20000	0.6077

Asymptotic Capacitance

N	k	Computed Value (μμF)
4, 6, 8	1.0	0.6001
4, 6, 8	0.1	0.6109

Table 8
The Semicircle: Radius = 1 cm
Exact Area: $0.15708 \times 10^{-3} m^2$

N	k	Area ($\times 10^{-3} m^2$)	Capacitance (μμF)
4	1.0	0.15307	0.4855
4	0.1	0.15616	0.5105
8	1.0	0.15607	0.5041
8	0.1	0.15537	0.5186

Table 9
The Quadrant
Radius = 1 cm

Exact Area: $0.78540 \times 10^{-4} m^2$

N	k	Area ($\times 10^{-4} m^2$)	Capacitance ($\mu\mu F$)
8	1.0	0.78413	0.3507
8	0.1	0.78273	0.3612

Table 10
The Sector of an Annulus: Radii: $R_1 = 1$ cm, $R_2 = 2$ cm

(a) Sector Angle: 180°

Exact Area:

		Area		
N	k	Computed ($\times 10^{-3} m^2$)	% Error	Capacitance ($\mu\mu F$)
8	1.0	0.45922	2.6	0.9456
8	0.8	0.45897	2.6	0.9502
8	0.1	0.53833	14.2	0.9399

(b) N = 4, k = 1.0

Sector Angle	Area			Capacitance ($\mu\mu F$)
	Computed ($\times 10^{-3} m^2$)	Exact ($\times 10^{-3} m^2$)	% Error	
180°	0.44534	0.47124	5.5	0.90000
120°	0.30000	0.31416	4.5	0.7113
90°	0.22961	0.23562	2.6	0.5994

Table 11
The Ellipse: Semi-Axes: a, b
N = 4, k = 1.0, b = 1 cm

Variation of Capacitance with a/b

a (cm)	Area (x 10^{-3} m^2)			Capacitance (μμF)		
	Computed	Exact	% Error	Computed	Exact	% Error
1.0	0.30615	0.31416	2.6	0.6695	0.70800	5.4
1.2	0.36737	0.37699	2.6	0.7350	0.77719	5.4
1.4	0.42860	0.43982	2.6	0.7980	0.84365	5.4
1.5	0.45922	0.47124	2.6	0.8288	0.87604	5.4
1.6	0.48983	0.50265	2.6	0.8591	0.90794	5.4
1.8	0.55106	0.56549	2.6	0.9185	0.9703	5.3
2.0	0.61229	0.62832	2.6	0.9766	1.0314	5.4
5.0	1.5307	1.5708	2.6	1.753	1.8436	4.9

Table 12
The Circle-with-Tangents: Tangent Angle (α) = 30°

Radius (cm)	N	k	Area (x 10^{-3} m^2)		Capacitance (μμF)
			Computed	Exact	
1	4	1.0	0.37320	0.38264	0.7509
	4	0.1	0.38202	0.38264	0.7869
2	8	1.0	1.5210	1.5306	1.553
	8	0.1	1.5144	1.5306	1.593

REFERENCES

[1] J. C. Maxwell (Ed.): "Electrical Researches," Cambridge University Press, 1879.

[2] D. Reitan and T. Higgins: "Accurate Determination of the Capactiance of a Thin Conducting Rectangular Plate," A.I.E.E. Trans., vol. 75, Pt. 1, 1957, pp. 761-766.

[2] R. F. Harrington: "Field Computation by Moment Methods," Macmillan Co., New York, 1968.

[4] B. Noble: "The Numerical Solution of the Singular Integral Equation for the Charge Distribution on a Flat Rectangular Lamina," PICC Symposium on Differential and Integral Equations, Rome, 1960.

[5] O. C. Zienkiewicz and D. V. Phillips: "An Automatic Mesh Generation Scheme for Plane and Curved Surfaces by 'Isoparametric Coordinates'," Intr. Jrnl. Num. Meth. Engng., 3, 1971, pp. 519-528.

[6] W. J. Gordon and C. A. Hall: "Construction of Curvilinear Coordinate Systems and Applications to Mesh Generation," Int. Jrnl. Num. Meth. Engng., 7, p. 973, pp. 461-477.

[7] J. Fukuda and J. Suhara: "Automatic Mesh Generation for Finite-Element Analysis," Advances in Computational Methods in Structural Mechanics and Design, (Ed. J. T. Oden, R. W. Clough and Y. Yamamoto), U.A.H. Press, Huntsville, Alabama, 1972, pp. 607-624.

[8] J. C. Cavendish: "Automatic Triangulation of Arbitrary Planar Domains for the Finite Element Method," Int. Jrnl. Num. Meth. Engng., 8, 1974, pp. 679-696.

[9] R. D. Shaw and R. G. Pitchen: "Modifications to the Suhara-Fukuda Method of Network Generation," Int. Jrnl. Num. Meth. Engng., 12 1978, pp. 93-99.

[10] I. Ergatoudis, B. M. Irons and O. C. Zienkiewicz: "Curved, Isoparametric, "Quadrilateral" Elements for Finite-Element Analysis," Int. Jrnl. Solids and Structures, 4, 1968, pp. 31-42.

[11] O. C. Zienkiewicz: "The Finite-Element Method in Engineering Science," McGraw-Hill, London, 1971.

[12] G. Steinmueller: "Restriction in the Application of Automatic Mesh Generation Schemes by 'Isoparametric Coordinates'," Int. Jrnl. Num. Meth. Engng., 8, 1974, pp. 289-294.

[13] A. K. Gupta: "A Finite Element for Transition from a Fine to a Coarse Grid," Int. Jrnl. Num. Meth. Engng., 12, 1978, pp. 34-45.

[14] W. J. Gordon: "Spline-blended Surface Interpolation through Curved Networks," J. Math. Mech. 18, 1969, pp. 931-952.

[15] W. J. Gordon: "Blending Function Methods of Bivariate and Multivariate Interpolation and Approximation," SIAM J. Num. Anal. 8, 1971, pp. 158-177.

[16] F. A. Akyuz: "Natural Coordinate Systems, An Automatic Input Data Generation Scheme for a Finite Element Method," Engng. and Design, 11, 1970, pp. 195-207.

[17] W. A. Cook: "Body Oriented (Natural) Coordinates for Generating Three-Dimensional Meshes," Int. Jrnl. Num. Meth. Engng., 8, 1974, pp. 27-43.

[18] A. Bykat: "Automatic Generation of Triangular Grid: I - Subdivision of a General Polygon into Convex Subregions. II - Triangulation of Convex Polygons," Int. Jrnl. Num. Meth. Engng., 10, 1976, pp. 1329-1342.

[19] J. C. Cavendish, C. A. Hall and O. C. Zienkiewicz: "Blended Infinite Elements for Parabolic Boundary Value Problems," Int. Jrnl. Num. Meth. Engng, 12, 1978, pp. 1841-1851.

[20] E. M. Deeley and E. E. Okon: "A Numerical Method of Solving Fredholm Integral Equations Applied to Current Distribution and Inductance in Parallel Conductors," Int. Jrnl. Num. Meth. Eng., 11, 1977, pp. 447-467.

[21] W. R. Smythe: "Static and Dynamic Electricity," McGraw-Hill, New York, 3rd Ed., p. 123.

[22] G. Strang and G. J. Fix: "An Analysis of the Finite Element Method," Prentice Hall, Englewood Cliffs, N. J., 1973.

[23] M. A. Eisenberg and L. E. Malvern: "On Finite-Element Integration in Natural Coordinates," Int. Jrnl. Num. Meth. Engng., I, 1973, pp. 574-575.

[24] N. Katz: "Integration of Triangular Finite Elements Containing Corrective Rational Functions," Int. Jrnl. Num. Meth. Engng., 11, 1977, pp. 107-114.

[25] P. Silvester: "Construction of Triangular Finite Element Universal Matrices," Int. Jrnl. Num. Meth. Engng., 12, 1978, pp. 237-244.

[26] E. Jahnke, F. Emde, and F. Losch: "Tables of Higher Functions," McGraw-Hill, New York, 6th Ed., 1960.

[27] M. Abramowitz and I. Stegun: "Handbook of Mathematical Functions," Dover, New York.

[28] C. Hastings: "Approximations for Digital Computers," Princeton University Press, 1955, pp. 172-175.

[29] F. de Meulenaere and J. Van Bladel: "Polarizability of Some Small Apertures," IEEE Trans. Ant. and Prop., vol. AP-25, March 1977, pp. 198-205.

APPENDIX

A-1. The Capacitance of an Ellipsoid

The capacitance C of an ellipsoid with semiaxes a, b, c is given by Smythe[21] as

$$C = 8\pi\varepsilon_o \Big/ \int_0^\infty \frac{dx}{\sqrt{(x + a^2)(x + b^2)(x + c^2)}} . \tag{A1}$$

In order to evaluate the integral in (1) we use the following result given by Jahnke, Emde and Losch[26]:

$$\int_x^\infty \frac{dt}{\sqrt{(b^2 + t^2)(c^2 + t^2)}} = \frac{1}{c} F(\phi,k), \tag{A2}$$

where $\cot \phi = x/c$, $k = \frac{1}{c}\sqrt{c^2 - b^2}$, $0 \le k \le 1$,

and $$F(\phi,k) = \int_0^\phi \frac{du}{\sqrt{1 - k^2 \sin^2 u}} ,$$

the incomplete elliptic integral of the first kind. Under the transformation $t^2 = x + c^2$, the integral in (A1) becomes

$$I = 2 \int_c^\infty \frac{dt}{\sqrt{(t^2 + a^2 - c^2)(t^2 + b^2 - c^2)}} ,$$

Using (2), and assuming that $a > b > c$, we obtain immediately

$$I = \frac{2}{\sqrt{a^2 - c^2}} F[\cot^{-1} \frac{c}{\sqrt{a^2 - c^2}}, \frac{\sqrt{a^2 - b^2}}{a^2 - c^2}].$$

The capacitance of the ellipsoid can, therefore, be expressed in the form

$$C = 4\pi\varepsilon_o(a^2 - c^2)^{1/2}/F[\sin^{-1}(1 - c^2a^{-2})^{1/2}, (a^2 - b^2)^{1/2}(a^2 - c^2)^{-1/2}] \quad (A3)$$

This expression corrects the result given by Smythe.[21]

The Ellipse

When $c = 0$, because $F(\pi/2,k) = K(k)$ (i.e., the complete elliptic integral of the first kind with modulus k), (A3) becomes

$$C = 4\pi a\varepsilon_o/K(e), \quad (A4)$$

where a is the semi-major axis of the ellipse and e the eccentricity.

For a circle of radius a, putting $a = b$ in (A4) gives immediately

$$C = 8a\varepsilon_o,$$

a well-known result.

A.2 The Potential due to a Uniform Charge Distribution Over a Triangle.

We present here a summary of the procedures adopted in deriving the relations (27) and (30) for the potential due to a uniform charge distribution over a triangle. The notation adhered to is that used in Section 4.2, unless otherwise indicated.

A.2.1 Field points in the plane of the triangle.

A.2.1.1 The ξ-Integral.

We have

$$g(x'_s,y'_s;\eta) = \int_0^1 \frac{(1-\eta)d\xi}{D\{x'_s,y'_s;x(\xi,\eta),y(\xi,\eta)\}} \qquad \text{(A-5)}$$

where

$$D\{x'_s,y'_s;x(\xi,\eta),y(\xi,\eta)\} = \sqrt{\{x(\xi,\eta) - x'_s\}^2 + \{y(\xi,\eta) - y'_s\}^2},$$

$$x(\xi,\eta) - x'_s = A_1\xi + B_1, \quad y(\xi,\eta) - y'_s = A_2\xi + B_2,$$

$$A_1 = a_{1rk}(1-\eta), \quad B_1 = b_{1rk}\eta + \bar{c}_{1rk}, \quad \bar{c}_{1rk} = c_{1rk} - x'_s$$

$$A_2 = a_{2rk}(1-\eta), \quad B_2 = b_{2rk}\eta + \bar{c}_{2rk}, \quad \bar{c}_{2rk} = c_{2rk} - y'_s.$$

We then have

$$D^2\{x'_s,y'_s,x(\xi,\eta),y(\xi,\eta)\} = (A_1^2 + A_2^2)\{(\xi + p')^2 + q^2\}$$

where

$$\alpha_{rk}^2(1-\eta)p' = \eta(a_{1rk}b_{1rk} + a_{2rk}b_{2rk}) + a_{1rk}\bar{c}_{1rk} + a_{2rk}\bar{c}_{2rk};$$

$$\alpha_{rk}^2(1-\eta)q = \eta(a_{1rk}b_{2rk} - a_{2rk}b_{1rk}) + a_{1rk}\bar{c}_{2rk} - a_{2rk}\bar{c}_{1rk}.$$

These relations give

$$\alpha_{rk}g(x'_s,y'_s;\eta) = \int_0^1 \frac{d\xi}{\sqrt{(\xi + p')^2 + q^2}},$$

i.e. $$\alpha_{rk}g(x'_s,y'_s;\eta) = \left[\cosh^{-1}\frac{\xi + p'}{q}\right]_0^1,$$

which is the same as (28).

A.2.1.2. The η-Integrals

In order to obtain (29) we require a primitive for

$$f(\eta) = \log\{a + b\eta + \sqrt{(a+b\eta)^2 + (c+d\eta)^2}\} - \log\{a'+b'\eta + \sqrt{(a'+b'\eta)^2 + (c+d\eta)^2}\}$$

It is easy to see that such a primitive has an algebraic form which does not depend on the sign of $(c + d\eta)$. Thus, provided $-c/d \notin [0,1]$, we may consider, instead, a primitive for the function

$$f'(\eta) = \log\{(\frac{a + b\eta}{c + d\eta}) + \sqrt{(\frac{a+b\eta}{c+d\eta})^2 + 1}\} - \log\{(\frac{a'+b'\eta}{c+d\eta}) + \sqrt{(\frac{a'+b'\eta}{c+d\eta})^2 + 1}\}$$

However, it can be shown that even when $-c/d \in [0,1]$, the improper integral $\int_0^1 f'(\eta)\, d\eta$ converges. It is, therefore, sufficient to obtain a primitive $E_1(a,b;\eta)$ for

$$\bar{f}(a,b;\eta) = \log\{(\frac{a + b\eta}{c + d\nu}) + \sqrt{(\frac{a + b\eta}{c + d\eta})^2 + 1}\}.$$

for the case $c + d\eta > 0$.

On writing $a + b\eta = (c + d\eta)\text{sh}\,\theta$, we find that

$$\int \bar{f}(a,b;\eta)\, d\eta = \frac{ad - bc}{d} [\frac{\theta}{d\text{sh}\theta - b} - \int \frac{d\theta}{d\text{sh}\theta - b}]$$

and it is easily shown that

$$\int \frac{d\theta}{d\text{sh}\theta - b} = \frac{1}{\sqrt{b^2 + d^2}} \log \left| \frac{d(\text{sh}\theta + \cosh\theta) - (b + \sqrt{b^2 + d^2})}{d(\text{sh}\theta + \cosh\theta) - (b - \sqrt{b^2 + d^2})} \right|,$$

so that

$$E_1(a,b,\eta) = E(a,b;\eta) + \frac{c + d\eta}{d} \log\,(c + d\eta).$$

A primitive for $\bar{f}(a',b';\eta)$ is

$$E_1(a',b';\eta) = E(a',b';\eta) + \frac{c + d\eta}{d} \log\,(c + d\eta)$$

Thus the required primitive for $f(\eta)$ is

$$E(\eta) = E(a,b;\eta) - E(a',b';\eta). \tag{A6}$$

This primitive yields the first expression for C_{srk} given in Section 4.2.

Alternative Expressions

We now consider alternative methods of simplifying the expression

$$H(a,b;\eta) = \log \left| \frac{d\{a + b\eta + \sqrt{(a+b\eta)^2 + (c+d\eta)^2}\} - (c+d\eta)(b+\sqrt{b^2+d^2})}{d\{(a+b\eta) + \sqrt{(a+b\eta)^2 + (c+d\eta)^2}\} - (c+d\eta)(b-\sqrt{b^2+d^2})} \right|$$

(i) Direct reduction

Now

$$H(a,b;\eta) = \log \left| \frac{d(\cosh\theta + \text{sh}\,\theta) - (b + \sqrt{b^2+d^2})}{d(\cosh\theta + \text{sh}\,\theta) - (b - \sqrt{b^2+d^2}} \right| .$$

Let

$$X_1 = d\cosh\theta + \sqrt{b^2+d^2}, \qquad Y_1 = d\cosh\theta - \sqrt{b^2+d^2},$$

$$\alpha_1 = d\,\text{sh}\,\theta + b, \qquad \beta_1 = d\,\text{sh}\,\theta - b.$$

Then $X_1Y_1 = \alpha_1\beta_1$.

Thus, $$H(a,b;\eta) = \log \left| \frac{Y_1 + \beta_1}{X_1 + \beta_1} \right| = \log \left| \frac{(Y_1 - \alpha_1)(Y_1 + \beta_1)}{(Y_1 - \alpha_1)(X_1 + \beta_1)} \right| ,$$

i.e. $$H(a,b;\eta) = -\log \left| \frac{X_1^2 - \beta_1^2}{\beta_1} \right| + \text{constant}.$$

On substituting for X_1 and β_1 and ignoring constants in the primitive from now on, we find that

$$H(a,b;\eta) = -\log \left| \frac{d + b\,\text{sh}\,\theta + \cosh\theta\sqrt{b^2+d^2}}{d\,\text{sh}\,\theta - b} \right| \tag{A7}$$

Since $(c + d\eta)(d\text{sh}\theta - b) = ad - bc$, a constant, we find, on simplifying the right-hand side of (A7) that

$$H(a,b;\eta) = -\log[(b^2+d^2)\eta + ab + cd + \sqrt{[(b^2+d^2)\eta+ab+cd\}^2 + (ad-bc)^2}] \qquad \text{(A8)}$$

(ii) The use of subsidiary integrals.

We obtain here two primitives $h_1(\eta)$ and $h_2(\eta)$ for the function

$$h(a,b;\eta) = \sqrt{(a+b\eta)^2 + (c+d\eta)^2}, \qquad \text{(A9)}$$

where

$$h_1(\eta) = \int (c+d\eta)\sqrt{\left(\frac{a+b\eta}{c+d\eta}\right)^2 + 1}\, d\eta$$

and

$$h_2(\eta) = \sqrt{b^2+d^2}\int \{\eta + \frac{ab+cd}{b^2=d^2}\}^2 + \{\frac{a^2+c^2}{b^2+d^2} - \frac{(ab+cd)^2}{(b^2+d^2)^2}\}\, d\eta$$

For $h_1(\eta)$, putting $a + b\eta = (c + d\eta)\sinh\theta$, as before, gives

$$h_1(\eta) = \frac{1}{2(b^2+d^2)}\{(b^2+d^2)\eta + ab + cd\}\sqrt{(a+b\eta)^2+(c+d\eta)^2}$$

$$-\frac{(ad-bc)^2}{2(b^2+d^2)^{3/2}}\log\left|\frac{d\{a+b\eta+\sqrt{(a+b\eta)^2+(c+d\eta)^2}\} - (c+d\eta)(b+\sqrt{b^2+d^2}}{d\{a+b\eta+\sqrt{(a+b\eta)^2+(c+d\eta)^2}\} - (c+d\eta)(b-\sqrt{b^2+d^2}}\right|.$$

When the integral for $h_2(\eta)$ is calculated, however, we have

$$h_2(\eta) = \frac{1}{2(b^2+d^2)}\{(b^2+d^2)\eta + ab + cd\}\sqrt{(a+b\eta)^2+(c+d\eta)^2}$$

$$+\frac{(ad-bc)^2}{2(b^2+d^2)^{3/2}}\log[(b^2+d^2)\eta+ab+cd+\sqrt{\{(b^2+d^2)\eta+ab+cd\}^2+(ad-bc)^2}]$$

These two expressions for the primitive of $h(a,b;\eta)$ thus establish the equivalence already implied by (A7) and (A8).

A.2.2 Arbitrary field points

A.2.2.1 The ξ-Integral

Here, instead of (A5), we have

$$\bar{g}(x_s',y_s',z_s';\eta) = \int_0^1 \frac{(1-\eta)\,d\xi}{\bar{D}\{x_s',y_s',z_s';x(\xi,\eta),y(\xi,\eta)\}},$$

where, on proceeding as in Section A.2.1.1 we find

$$\alpha_{rk}\bar{g}(x_s',y_s',z_s';\eta) = \int_0^1 \frac{d\xi}{\sqrt{(\xi+p')^2+\bar{q}^{-2}}}$$

where $\bar{q}^{-2} = q^2 + \frac{e^2}{(1-\eta)^2}$, and $\alpha_{rk}^2 e^2 = z_s'^2$.

Thus,

$$\alpha_{rk}\bar{g}(x_s',y_s',z_s';\eta) = \log\{a+b\eta+\sqrt{(a+b\eta)^2+(c+d\eta)^2+e^2}\}$$
$$-\log\{a'+b'\eta+\sqrt{(a'+b'\eta)^2+(c+d\eta)^2+e^2}\},$$

with a, b, a', b', c, d, being defined as in Section A.2.1.1

A.2.2.2 The η-Integral

(i) The p-η transformation and applications

We define a new variable p as follows:

$$p = \sqrt{(c+d\eta)^2+e^2}\ .$$

This allows us to proceed as in Section A.2.1.2, so that we need only consider the primitive of the function

$$\bar{f}'(a,b;\eta) = \log\{(\frac{a+b\eta}{p}) + \sqrt{(\frac{a+b\eta}{p})^2+1}\}.$$

The relation

$$a + b\eta = p\ \mathrm{sh}\ \phi$$

gives

$$pd \text{ sh } \phi = k + b\sqrt{p^2 - e^2}, \qquad k = ad - bc,$$

so that p satisfies the x-quadratic

$$x^2(d^2 \text{sh}^2 \phi - b^2) - 2xdk\text{sh } \phi + b^2e^2 + k^2 = 0.$$

We choose the root p given by

$$up = dk \text{ sh } \phi + b\sqrt{k^2 - e^2u}, \tag{A-10}$$

where $u = d^2\text{sh}^2 \phi - b^2$, since this expression for p reduces to $c + d\eta$ for field points which lie in the plane of the triangle (i.e. for $e = 0$).

The primitive for $f'(a,b;\eta)$ is thus

$$G(a,b;\eta) = \phi\eta - \int \eta \, d\phi.$$

Since $b\eta = -a + p \text{ sh } \phi$, we have

$$G(a,b;\eta) = G_o - \frac{k}{b} G_1 + G_2,$$

where

$$G_0 = \frac{\phi \, p \text{ sh } \phi}{b}, \quad G_1 = \frac{\phi}{d} + \frac{b^2}{d} \int \frac{d\phi}{d^2\text{sh}^2 \phi - b^2},$$

and

$$G_2 = \int \frac{\text{sh}\phi \sqrt{k^2 - e^2u}}{u} \, d\phi$$

Let

$$X = d \text{ sh } \phi + \sqrt{b^2 + d^2}, \qquad Y = d \text{ sh } \phi - \sqrt{b^2 + d^2},$$

$$\alpha = d \text{ sh } \phi + b, \qquad \beta = d \text{ sh } \phi - b \tag{A11}$$

Then $XY = \alpha\beta$, and we find that on writing

$$G_1 = \frac{\phi}{d} + \frac{b^2}{d} \bar{G}_1,$$

$$\bar{G}_1 = \int \frac{d\phi}{d^2\text{sh}^2 \phi - b^2} = \frac{1}{2b\sqrt{b^2 + d^2}} \left[\log \frac{Y + \beta}{X + \beta} - \log \frac{Y + \alpha}{X + \alpha}\right],$$

and

$$G_2 = \frac{e^2}{2d}\int \frac{du}{\sqrt{(k^2 - e^2u)(b^2+d^2+u)}} - \frac{k^2}{2d}\int \frac{du}{\sqrt{(k^2 - e^2u)(b^2+d^2+u)}}\cdot$$

It can be readily verified that

$$\int \frac{du}{\sqrt{(k^2 - e^2u)(b^2+d^2+u)}} = \frac{e}{d}\sin^{-1}\left[e\ \frac{b^2+d^2+u}{k^2+e^2(b^2+d^2)}\right],$$

and

$$\int \frac{du}{u\sqrt{(k^2 - e^2u)(b^2+d^2+u)}} = -\frac{1}{k\sqrt{b^2+d^2}}\log\left|\frac{k\sqrt{b^2+d^2+u}+\sqrt{b^2+d^2}\sqrt{k^2-e^2u}}{k\sqrt{b^2+d^2+u}-\sqrt{b^2+d^2}\sqrt{k^2-e^2u}}\right| \tag{A12}$$

These results ultimately show that

$$G(a,b;\eta) = \frac{(c+d\eta)\phi}{d} + \frac{k}{2d\sqrt{b^2+d^2}}\left[\log\left|\frac{Y+\alpha}{X+\alpha}\right| - \log\left|\frac{Y+\beta}{X+\beta}\right|\right]$$

$$+ \frac{e}{d}\sin^{-1}\left[\frac{ed\cosh\phi}{\sqrt{k^2+e^2(b^2+d^2)}}\right]$$

$$+ \frac{k}{2d\sqrt{b^2+d^2}}\log\left|\frac{kd\cosh\phi+\sqrt{b^2+d^2}\sqrt{k^2-e^2u}}{kd\cosh\phi-\sqrt{b^2+d^2}\sqrt{k^2-e^2u}}\right|, \tag{A13}$$

where $\phi = \log\left[\frac{a+b\eta+\sqrt{(a+b\eta)^2+(c+d\eta)^2+e^2}}{\sqrt{(c+d\eta)^2+e^2}}\right]$.

(ii) Alternative expressions

The expression $L = L_1 - L_2 + L_3$ occurs in (A13), where

$$L_1 = \log \left| \frac{Y + \alpha}{X + \alpha} \right|, \tag{A14}$$

$$L_2 = \log \left| \frac{Y + \beta}{X + \beta} \right|, \tag{A15}$$

and

$$L_3 = \log \left| \frac{kd \cosh \phi + \sqrt{b^2 + d^2}\ \sqrt{k^2 - e^2 u}}{kd \cosh \phi - \sqrt{b^2 + d^2}\ \sqrt{k^2 - e^2 u}} \right| \tag{A-16}$$

We give here a simplified form of L which is similar to the expression $H(a,b;\eta)$ defined by (A8).

(a) Direct reduction

Let $y = \sqrt{(a + b)^2 + (c + d)^2 + e^2}$.

It is easy to write (A16) in the alternative form

$$L_3 = L_{31} + L_{32}, \tag{A17}$$

where

$$L_{31} = \log \left| \frac{p\ \sqrt{b^2 + d^2}\ (b \cosh \phi + \sqrt{b^2 + d^2}\ \mathrm{sh}\phi) - kd}{p\ \sqrt{b^2 + d^2}\ (b \cosh \phi - \sqrt{b^2 + d^2}\ \mathrm{sh}\phi) + kd} \right|,$$

and

$$L_{32} = \log \left| \frac{\sqrt{b^2 + d^2}\ \mathrm{sh}\ \phi - b \cosh \phi}{\sqrt{b^2 + d^2}\ \mathrm{sh}\ \phi + b \cosh \phi} \right|.$$

A further reduction gives

$$L_{31} = p(a,b;\eta) - \log \{k^2 + e^2(b^2 + d^2)\},$$

where $$P(a,b;\eta) = 2 \log [(b^2 + d^2)\eta + ab + cd + y\sqrt{b^2 + d^2}], \tag{A18}$$

and $$y\sqrt{b^2 + d^2} = \sqrt{\{(b^2 + d^2)\eta + ab + cd\}^2 + (ad - bc)^2 + e^2(b^2 + d^2)}$$

Using the relations (A11) it is easy to show that

$$L_{32} = \log \left| \frac{X\beta - Y\alpha}{X\alpha - Y\beta} \right| , \tag{A19}$$

$$L_1 + L_2 = \log \left| \frac{Y}{X} \right| ; \tag{A20}$$

and that $L_1 - L_2 + L_{32} = \log \left| \dfrac{\sqrt{b^2 + d^2} - 2b}{\sqrt{b^2 + d^2} + 2b} \right|$, a constant.

We thus have immediately

$$L_1 - L_2 + L_3 = P(a,b;\eta) + \text{constant}, \tag{A21}$$

so that the function $L_1 - L_2 + L_3$, being a component of the primitive $G(a,b;\eta)$ given by (A13), is equivalent to $P(a,b;\eta)$. The function $P(a,b;\eta)$ is very similar to $H(a,b;\eta)$, and reduces to it when $e = 0$.

Reduced expressions for L_1, L_2 and L_3

The relations (A17) - (A21) imply that, to within arbitrary constants,

$$L_1 = \frac{1}{2} \log \left| \frac{\alpha^2 - Y^2}{X^2 - \alpha^2} \right| , \quad L_2 = \frac{1}{2} \log \left| \frac{\beta^2 - Y^2}{X^2 - \beta^2} \right| , \quad \text{and}$$

$$L_3 = P(a,b;\eta) + \log \left| \frac{\sqrt{b^2 + d^2}\ \operatorname{sh}\phi - b \cosh\phi}{\sqrt{b^2 + d^2}\ \operatorname{sh}\phi + b \cosh\phi} \right| .$$

On substituting for X, Y, α, β, ϕ and P, the following explicit reduced forms result:

$$L_1 = \log \left| \frac{b(a + b\eta) - d\sqrt{(c + d\eta)^2 + e^2} + y\sqrt{b^2 + d^2}}{d(a + b\eta) + b\sqrt{(c + d\eta)^2 + e^2}} \right| \tag{A22a}$$

$$L_2 = \log \left| \frac{d(a + b\eta) - b\sqrt{(c+d\eta)^2 + e^2}}{b(a+b\eta) + d\sqrt{(c+d\eta)^2 + e^2} + y\sqrt{b^2+d^2}} \right|, \qquad \text{(A22b)}$$

and

$$L_3 = 2 \log[(b^2 + d^2) + ab + cd + y\sqrt{b^2 + d^2}]$$
$$+ \log \left| \frac{b^2\{(c + d\eta)^2 + e^2\} - d^2(a + b\eta)^2}{(2b^2 + d^2)(a+b\eta)^2 + b^2\{(c+d\eta)^2 + e^2\} + 2b(a+b\eta)y\sqrt{b^2+d^2}} \right|. \qquad \text{(A22c)}$$

(b) Auxiliary integrals

In line with the procedure based on the function $h(a,b;\eta)$ defined by (A9), we consider here two primitives for the function

$$J(a,b;\eta) = \sqrt{(a + b\eta)^2 + (c + d\eta)^2 + e^2},$$

where the primitives $J_1(\eta)$ and $J_2(\eta)$ are given by

$$J_1(\eta) = \int p\sqrt{\left(\frac{a + b\eta}{p}\right)^2 + 1}\ d\eta;$$

$$J_2(\eta) = \sqrt{b^2 + d^2} \int \sqrt{\{\eta + \frac{ab + cd}{b^2 + d^2}\}^2 + \{\frac{a^2 + c^2}{b^2 + d^2} - \frac{(ab + cd)^2}{(b^2 + d^2)^2} + \frac{e^2}{b^2 + d^2}\}}$$

With the expression for p given by (A10), we find that

$$J_1(\eta) = \frac{a + b\eta}{2b}\sqrt{(a + b\eta)^2 + (c + c\eta)^2 + e^2}$$
$$+ \frac{(k^2 - b^2e^2)}{2b} \int \frac{d\theta}{d^2 sh^2\theta - b^2} + bk^2 \int \frac{d\theta}{(d^2 sh^2\theta - b^2)^2}$$
$$+ \frac{k^2}{2d} \int \frac{du}{u^2\sqrt{(b^2 + d^2 + u)(k^2 - e^2u)}} - \frac{e^2}{2d} \int \frac{du}{u\sqrt{(b^2 + d^2 + u)(k^2 - e^2u)}}$$

It is easy to show that

$$\int \frac{du}{u^2\sqrt{(b^2+d^2+u)(k^2-e^2u)}} = -\frac{1}{k^2u(b^2+d^2)}\cdot\sqrt{(b^2+d^2+u)(k^2-e^2u)}$$

$$+\frac{(k^2-b^2e^2-d^2e^2)}{4dk(b^2+d^2)^{3/2}}\log\left|\frac{k\sqrt{b^2+d^2+u}+\sqrt{b^2+d^2}\sqrt{k^2-e^2u}}{k\sqrt{b^2+d^2+u}-\sqrt{b^2+d^2}\sqrt{k^2-e^2u}}\right|$$

$$\int \frac{d\theta}{(d\,\mathrm{sh}\,\theta+b)^2} = -\frac{d\cosh\theta}{\alpha(b^2+d^2)}+\frac{bL_1}{(b^2+d^2)^{3/2}},$$

$$\int \frac{d\theta}{(d\,\mathrm{sh}\,\theta-b)^2} = -\frac{d\cosh\theta}{\beta(b^2+d^2)}-\frac{bL_2}{(\beta^2+d^2)^{3/2}}.$$

These relations, together with (A12), give the primitive

$$J_1(\eta) = \frac{\{(c+d\eta)(b^2+d^2)+kb\}}{2b(b^2+d^2)}\sqrt{(a+b\eta)^2+(c+d\eta)^2+e^2}$$

$$+\frac{\{k^2+e^2(b^2+d^2)\}}{4(b^2+d^2)^{3/2}}[L_1-L_2+L_3].$$

However, on evaluating the integral for $J_2(\eta)$, we find

$$J_2(\eta) = \frac{\{(c+d\eta)(b^2+d^2)+kb)\}}{2b(b^2+d^2)}\sqrt{(a+b\eta)^2+(c+d\eta)^2+e^2}$$

$$+\frac{\{k^2+e^2(b^2+d^2)\}}{4(b^2+d^2)^{3/2}}\,P(a,b;\eta).$$

Thus $L_1 - L_2 + L_3$ is equivalent to $P(a,b;\eta)$, as before.

A.2.2.3 Planar Interactions

The primitive $G(a,b;\eta)$ given by (A13) can be written in the form

$$G(a,b;\eta) = \frac{(c + d\eta)\phi}{d} + \frac{e}{d} \sin^{-1} \left[\frac{ed \cosh \phi}{\sqrt{k^2 + e^2(b^2 + d^2)}}\right]$$

$$+ \frac{k}{2d\sqrt{b^2 + d^2}} [L_1 - L_2 + L_3].$$

For planar interactions, $e = 0$, so that $X = X_1$, $Y = Y_1$, $\alpha = \alpha_1$, $\beta = \beta_1$ and $\phi = \theta$. Also,

$L_3 = \log \left| \frac{X_1}{Y_1} \right|$, and $L_1 + L_3 = \log \left| \frac{X_1 + \beta_1}{Y_1 + \alpha_1} \right|$, so that

$L_1 - L_2 + L_3 = -2L_2$, a relation which can also be established using the explicit forms given by (A22).

Thus, $G(a,b;\eta) = E_1(a,b;\eta)$, showing that when the field point lies in the plane of the uniformly charged triangle, we recover the primitive for planar interactions given by (A6).